Journal of Materials Chemistry B

ROYAL SOCIETY OF CHEMISTRY

PAPER

View Article Online
View Journal | View Issue

Cite this: J. Mater. Chem. B, 2025, 13, 3094

Mesoporous polymeric nanoparticles for effective treatment of inflammatory diseases: an *in vivo* study†

Divya Pareek,[a] Md. Zeyaullah,[b] Sukanya Patra,[a] Oviya Alagu,[a] Gurmeet Singh,[a] Kirti Wasnik,[a] Prem Shankar Gupta[a] and Pradip Paik *[a]

Acute inflammatory diseases require suitable medicine over the existing therapeutics. In this line, the present work is focused on developing polymeric nanomedicine for the treatment of inflammatory disorders. Herein, cell viable nanoparticles (GlyNPs) of size 180–250 nm in diameter and pore size of 4–5 nm in diameter, based on glycine and acryloyl chloride, have been developed and proved to be a potential anti-inflammatory agent without using any conventional drugs. These particles exhibit colloidal stability (with a zeta potential of −35.6 mV). A network pharmacology-based computational study has been executed on 9076 genes and proteins responsible for inflammatory diseases, out of which 10 are selected that have a major role in rheumatoid arthritis (RA). *In silico* docking study has been conducted to find out the targeted efficiency of the GlyNPs considering 10 inflammation-specific markers, namely IL-6, IL-1β, TNF-α, TLR-4, STAT-1, MAPK-8, MAPK-14, iNOS, NF-κβ and COX-2. The results revealed that the GlyNPs could be an excellent anti-inflammatory component similar to aspirin. The *in vitro* inflammation activity of these GlyNPs has also been checked on an inflammation model generated by LPS in RAW 264.7 macrophages. Then, the *in vitro* anti-inflammation efficiency has been checked with 10–150 μg mL^{-1} of GlyNP doses. The treatment efficiency has been checked on inflammation-responsible immune markers (NO level, NF-κβ, INF-γ, IL-6, IL-10, and TNF-α) and it was found that the GlyNPs are an excellent component in reducing inflammation. The *in vivo* therapeutic response of GlyNPs on the induced rheumatoid arthritis (RA) model has been evaluated by measuring the morphological, biochemical and immune-cytokine and interferon levels responsible for the inflammation, using a 2 g kg^{-1} dose (sample to weight of rat). The anti-inflammatory efficiency of GlyNPs without using additional drugs was found to be excellent. Thus, GlyNPs could be paramount for the potential treatment of various inflammatory diseases.

Received 7th September 2024,
Accepted 22nd January 2025

DOI: 10.1039/d4tb02012j

rsc.li/materials-b

1. Introduction

Acute inflammatory diseases are relatively common and can affect people of all ages.[1] Inflammation causes rheumatoid arthritis (RA), inflammatory bowel disease, psoriasis, and systemic lupus erythematosus.[2] Furthermore, inflammation can cause tissue damage, organ dysfunction, and numerous organ damage.[3,4] Researchers are continuing to explore new medicines to suppress inflammation. For example, the development of targeted immunotherapies is gaining traction, emphasizing the need for strategies that can both mitigate inflammatory processes and enhance patient recovery outcomes.[5] However, a comprehensive understanding of the inflammatory pathways involved in these diseases is required to identify immunotherapeutic targets.[6] Over the past three decades, advancements in treating inflammation have gained limited success, using molecular medicine. However, their cellular mechanism and therapeutic strategies are complicated.[7] The strategies involved specific inflammatory cytokines, gene therapies that modulate immune responses, and drug delivery systems based on anti-inflammatory agents.[7] These therapies specifically target the biomarker molecules intricate in the inflammatory process. Although these treatment procedures improved the quality of life for many patients to some extent by reducing symptoms, they showed severe side effects.[8] Hence, it is urgent to develop suitable medicines to reduce inflammation and resolve the associated issues. Targeted therapies, for example,

[a] School of Biomedical Engineering, Indian Institute of Technology, Banaras Hindu University (BHU), Varanasi, Uttar Pradesh 221 005, India. E-mail: paik.bme@iitbhu.ac.in, pradip.paik@gmail.com
[b] Department of Zoology, Banaras Hindu University (BHU), Varanasi, Uttar Pradesh 221005, India

† Electronic supplementary information (ESI) available. See DOI: https://doi.org/10.1039/d4tb02012j

cell-depleting monoclonal antibodies, rituximab (anti-CD20) and alemtuzumab (anti-CD52), were used against other inflammatory diseases, including RA.[9] Anti-cytokine therapies targeting specific inflammatory pathways, *e.g.*, TNF-α, IL-12, IL-17, IL-23, and IL-35-based therapies, have also been reported.[10] Similarly, bispecific antibodies and nanobodies,[11] *i.e.*, recombinant variable domains of heavy chain-only antibodies (which make them effective for therapeutic applications), were also used to target multiple immune mediators and gene therapy approaches to reduce inflammation.[2] However, these treatment approaches required surgical interventions, several challenges persist, and the high cost limits access for many patients.

Many nanomaterial-based approaches are also used for the treatment of inflammatory diseases.[12] Nanoparticles can be designed to target specific cells and tissues involved in inflammation, such as activated macrophages or endothelial cells, present at the site of inflammation.[13] Steroid/non-steroid/peptide/biomimetic-based nanoparticles were also reported for anti-inflammation purposes.[14] Inorganics such as Au, Ag, ZnO, SiO_2, TiO_2, CdO, ZnO, Fe_2O_3 *etc.* NPs are reported for treating inflammatory diseases due to their catalytic properties and ability to directly react to neutralize reactive oxygen/nitrogen species (ROS/RNS) and inhibit the pro-inflammatory cytokines, such as IL-6, INF-γ and TNF-α that drive inflammation by promoting the levels of anti-inflammatory cytokines like IL-4 and IL-10.[14,15] Anti-inflammatory drug-loaded nanoparticles are also reported to reduce chronic inflammation,[14] such as CeO_2 loaded with enzyme,[16] PEGylated Pt NPs[16] tannic-acid mineral nanoparticles (TMPs) assembled with bioactive calcium and phosphate ions reported for their use in anti-inflammation.[17] Although inorganic NPs were used for treating inflammation, their potential to induce inflammation, variability in immune response, and toxicity concerns must be carefully addressed before successful clinical implementation.[15] On the other hand, a few polymeric nanoparticles, such as PEGylated liposomes,[18] hyaluronic acid-coated solid lipid NPs,[19] PCL,[20] PEG-*b*-PLA micelles,[21] poly(NIPAm-*co*-AMPS),[22] and chitosan/poly(γ-glutamic acid)[23] *etc.* are also reported for the treatment of inflammatory disorders.[14] There is also an increasing trend to load anti-inflammatory drugs in polymeric nanoparticles and deliver the same to resolve inflammatory diseases.[24] Despite that, there is huge concern about the biodistribution, pharmacokinetics and toxicity of drugs in resolving inflammation-related issues.[24] All these medicines limit their use with secondary infections due to the lack of specificity.[1] Earlier, we have used glycine and acryloyl chloride-based functional polymeric nanoparticles/nanocapsules without using/loading any conventional drugs for wound healing. However, without loading, no anti-inflammatory drugs/steroids have ever been reported as anti-inflammatory agents for the treatment of RA. These polymeric nanocapsules could be promising therapeutics for the effective treatment of inflammatory diseases such as RA, which is the main focus of this work. There is a lot of scope to improve in this direction.

In the above line, the present work focused on developing mesoporous polymeric nanoparticles (GlyNPs) based on glycine and acryloyl chloride. These NPs were qualified for therapeutic applications through the cell viability study on RAW 264.7 macrophage and PC-12 cell lines with varying concentrations, studying the cellular uptake on RAW 264.7 macrophages. Then, a network pharmacology-based computational study was accomplished to find out the genes and proteins responsible for the major inflammatory diseases, for example RA. Subsequently, *in silico* docking study has been conducted to find out the targeted efficiency of the synthesized polymeric particles considering ten inflammation-specific markers (*e.g.*, IL-6, IL-1β, TNF-α, TLR-4, STAR-1, MAPK-8, MAPK-14, iNOS, NF-κβ and COX-2) and the results have been compared with the commercially available standard anti-inflammatory drugs (aspirin and diclofenac). Based on the computational results, the efficiency of the synthesis of polymeric partials has been authenticated in an *in vitro* study by varying the doses of novel polymeric NPs and the inflammation levels of a few immune markers (NO, NF-κβ, INF-γ, IL-6, IL-10, and TNF-α) were verified to be responsible for the inflammation. After receiving the progressive *in vitro* therapeutic response of the novel polymeric NPs, the work has been extended to an *in vivo* pristane-induced RA rat model to check the therapeutic proficiency of the synthesized GlyNPs without loading any additional drugs. Then, the *in vivo* therapeutic efficiency was evaluated by studying the morphology of the rat's paws and ankles, biochemical analysis by blood serum, and immune parameters using ELISA assay. Finally, the effective therapeutic potential of the synthesized glycine-acryloyl chloride-based GlyNPs to control inflammation without using any conventional drug has been established.

2. Experimental methods

2.1 Materials

The following materials were used: Glycine (98%, Sigma Aldrich, Germany), potassium hydroxide (KOH) (Merck), 1,4-dioxane (99%) (Merck), acryloyl chloride stabilized with 400 ppm phenothiazines (96%, Thermofisher-scientific), magnesium sulphate anhydrous (SRL), trimethylamines (≥ 99.5%, Merck), SDS (sodium dodecyl sulphate) (90%, Merck), hexadecane anhydrous (99%, Sigma Aldrich, Germany), divinylbenzene (DVB) (Alfa-Aesar), ethyl acetate, chloroform, and 1,4-dioxane (99% pure, Merck). 2,2-Azobisisobutyronitrile (AIBN) (98%, SRL), dichloromethane, *n*-hexane, hydrochloric acid, diethyl ether, dichloromethane, sodium bisulphate, sodium chloride, toluene, DMSO-d_6, $CdCl_3$, phosphate buffered saline (PBS) (pH 7.4), isopropanol, phosphotungstic acid, DNS (sodium chloride and dextrose injection IP (0.9% and 5% w/v)) (Jedux), DMEM Cell Clone, fetal bovine serum (Gibco), penicillin–streptomycin cocktail and gentamicin (Himedia), methyl thiazole tetrazolium (MTT), DMSO (Merck), DABCO (Sigma Aldrich), rhodamine B (Sigma), Hoechst 33258 (Cyamann), Nile red (SRL), Quanti blue (Invivogen), Griess reagent (Biotium) and DAPI (Invitrogen). These chemicals were used as received commercially. All samples were prepared using ultrapure water (18.2 MΩ cm) (Sisco Research Laboratories Pvt. Ltd, Mumbai, India).

2.2 Methods

Synthesis of the *N*-acryloyl glycine monomer (NAG). *N*-Acryloyl glycine monomer was synthesized by modifying our previously reported protocol.[25] In brief, two separate solutions were prepared: solution 'A' consisting of 2 gm glycine dissolved in 2 M KOH and solution 'B' with ~3 g acryloyl chloride in 1,4-dioxane. Both solutions were placed in an ice bath. Solution 'B' was then added to solution 'A' dropwise, and then the pH of the mixture was adjusted to 12 by adding KOH (2 M) dropwise. The new mixture was stirred for 2 h at 600 rpm at room temperature (25 °C). Then, the solution was washed thrice with ethyl acetate using a separating funnel. Then, the obtained solution was saturated with excess NaCl, and its pH was reduced to 2 using HCl (5 M). The aqueous solution that was obtained was again washed with diethyl ether. The organic layer of ethyl acetate was collected and dried with $MgSO_4$ (anhydrous) and filtered. Then, the monomer was extracted by vacuum evaporation through a rotary evaporator. Finally, ethyl acetate and diethyl ether (1 : 1) were used to recrystallise the solid *N*-acryloyl glycine monomer (NAG). The yield of the product was obtained to be 63.75%.

Synthesis of glycine nanoparticles (GlyNPs). In brief, *N*-acryloyl glycine monomer (500 mg) was taken in 4 mL toluene. A 50 mg AIBN as a radical initiator, 30 μL hexadecane as a co-stabilizer and 50 μL divinyl benzene (DVB) as a cross-linking agent were added. Then, a solution of SDS (60 mg dissolved in 2 mL H_2O) was added. Finally, the mixture was sonicated for 5 minutes at 25 °C (ultra-probe syndicator, 750 W, 30% power, 45 s of sonication followed by 15 s intervals) to form the emulsion. Then, the emulsion was heated at 80–85 °C for 12–18 h with continuous stirring at 600 rpm to ensure complete polymerization. This process resulted in the formation of stable nanoparticles. The obtained GlyNPs suspension was washed with water–ethanol mixture (50 : 50) repeatedly (5–7 times) through centrifugation (15 000 rpm at 4 °C) with a 45-minute cycle followed by lyophilization. Then, the solid white sample was stored for further studies.

2.3 Characterization of the GlyNPs

The chemical functionality of the monomer and the polymers was characterized through FTIR (Nicolet iS5, 4 Thermo Fisher Scientific Inc., USA) (with KBr pellet), ^{1}H-NMR and ^{13}C-NMR (Model: AVH D 500 AVANCE III HD 500 MHz One Bay NMR Spectrometer, BRUKER BioSpin International AG spectrometer, solvent DMSO-d_6).

The morphology and size of the polymer particles was checked through HRTEM (Tecnai G2 20 TWIN, FEI Company of USA (S.E.A.) PTE, LTD), AFM (NTEGRA Prima, NT-MDT Service & Logistics Ltd) and dynamic light scattering (DLS; Nano-ZS ZEN3600, Malvern, UK) at 25 °C. The zeta potential (ζ) was calculated with the comprehensive option attached to the DLS.

2.4 Biological study of GlyNPs

All cell-based experiments were performed using RAW264.7 (monocyte macrophages) cell lines, and neural crest-originated catecholamine PC12 cells (pheochromocytoma) were obtained from the National Centre for Cell Science, Pune, India. All cells were cultured using DMEM-high glucose media (4.5 g L^{-1}) containing sodium pyruvate and sodium bicarbonate (Sigma-Aldrich), supplemented with FBS (10 vol%) and penicillin and streptomycin cocktail (1 vol%), in a CO_2 incubator at 37 °C with 5% CO_2. Cell lines were cultured in tissue culture T-75 flasks (gentix), and the culture medium was changed every alternate day.

Cell culture and cell viability. *In vitro* cell viability of GlyNPs was studied using RAW264.7 macrophages and PC-12 cell lines with varying concentrations of NPs. Cell viability was studied using an MTT assay. In brief, both the cell lines were seeded at 1×10^4 cells per well into a 96-well plate and kept for 24 h to allow their adhesion to the walls. GlyNPs of varying concentrations (10, 20, 40, 80, 100, 125, 150, 200 and 250) μg mL^{-1} (dispersed in a complete culture medium) were added to each well and incubated for 24 h. Then, the particle-treated media was removed, and MTT solution (5 mg mL^{-1}) prepared in fresh complete media was added, followed by 4 h incubation at 37 °C. Finally, the MTT solution was removed, and then 100 μL of DMSO in each well was added and incubated for 30 min. Afterwards, it was incubated in the dark to dissolve the formazan crystals. Finally, a microplate reader acquired the absorbance at λ_{max} = 570 nm (Biotech). The percentage of cell viability (%) was calculated using eqn (1).

$$\%\ \text{Cell viability} = \frac{\text{OD (treatment)}}{\text{OD (Control)}} \times 100 \qquad (1)$$

All the experiments were conducted in triplicate and represented with statistical errors.

Cellular uptake. To study the cellular uptake of GlyNPs, RAW 264.7 macrophages (1×10^6 per well) were used. Cells were cultured on a lysine-coated glass coverslip with 2 mL of complete media in a 6-well plate and incubated for 24 h to reach 70–80% confluency with adhesion. The GlyNPs were stained with Nile red for 24 h. Furthermore, the prepared GlyNPs stained with Nile red taken in 100 μg mL^{-1} complete media were added to each well and incubated for another 24 h. Then, the cells were washed with PBS (pH 7.4) three times to remove any unbound GlyNPs. Then, the cells were fixed with 400 μL of 4% paraformaldehyde solution per well and kept for 30 min. Then, the cells were stained with DAPI. Each coverslip was placed upon a glass slide using the mounting agent Dabco. The images were acquired through Confocal microscopy (Leica Super-resolution SP8 (BHU-SATHI)) to observe the localization of the GlyNPs. Then, the images were analysed using Image J Fiji Software.

2.5 *In silico* studies

To investigate the potential uses of GlyNPs, several *in silico* studies were carried out. First, network pharmacology predictions applying various important molecular targets associated with anti-inflammatory capacity were identified. Next, molecular docking was performed to examine the interactions between the GlyNPs and the identified target proteins. Then, using the computational results, we illuminated the potential mechanisms

Table 1 The forward and reverse primer sequences of all the genes used for RT-PCR

Marker	Forward (5′ to 3′)	Reverse primer (3′ to 5′)	Amplicon size
IFN-γ	GAAAGGATGCATTCATG	AAAATTCAAAATAGTGCT	205
IL-6	ACAAGAAAGACAAGCCAG	GTCTATTCGACCTCAGTGT	145
TNF-α	CCACAAGCAGGAATGAG	AAAGACCTCCCTCTACAC	140
IL-10	AAAATAAGAGCAAGGC	GTATGCAAATTCATTG	82
GAPDH	TGGGAGTTGCTGTTGAAGCG	GGTGGAAGAACTACAGT	103

of action, therapeutic efficacy, and specificity of the GlyNPs for biological applications. All the software tools used for computational purposes are enlisted (in Table 1 with web references).

Network pharmacology. In our earlier report, glycine was used to prepare NAGA (poly(*N*-acryloyl glycine)) NPs with a size below 50 nm and used in wound healing and an anti-inflammatory response was observed.[26] In this alignment, we have chosen rheumatoid arthritis (RA) as a model target for inflammatory disease for the present study. Herein, the network pharmacology approach has been utilized to understand the potential target genes responsible for the inflammation. For this purpose, we have used three separate databases: GeneCards, DisGeNET, and MalaCards (Table S1, ESI†). Additionally, common potential target genes for the illness were investigated using a Venn diagram (Table S1, ESI†). To conduct a thorough investigation into the potential modulatory effects of our GlyNPs on proteins associated with rheumatoid arthritis, approximately 9076 target genes were selected. Then, the protein–protein interactions (PPI) were analysed using the retrieval of the Interacting Genes (STRING) database (Table S1, ESI†) in homo-sapiens specification. The PPI network was scrutinized using Cytoscape software. Then, we examined the hub genes in the PPI network using CytoHubba's Maximal Clique Centrality (MCC) technique.[27] All finalized gene sets were examined in shinyGO 0.80 to identify the biological processes, molecular functions and KEGG pathways impacted by compound–target interactions.

Molecular docking. The targeted gene was sorted out through a network pharmacology approach, and a molecular docking study was performed. The following are the major steps used for docking.

(a) Protein preparation. For docking, the following receptors were selected: COX2 (pdb id 6COX), NFκβ (pdb id ILE5), IL-6 (pdb id 1ALU), IL-1β (pdb id 5I1B), TNF-α (pdb id 2AZ5), iNOS (pdb id 4NOS), TLR-4 (pdb id 2Z62), MAPK-14 (pdb id 4F9Y), MAPK-8 (pdb id 4G1W), and STAT-1 (pdb id 3WWT). The 3D structures of the chosen receptors were retrieved from the RCSB protein Data Bank (**https://www.rcsb.org/**). Subsequently, water molecules were removed using Autodock 4.2.6, adding polar hydrogen and Kollman's charges. The resulting proteins were then saved in PDBQT format.

(b) Ligand preparation. Molecular docking studies were conducted using AutoDock 4.2 software. For this study, the ligands selected were *N*-acryloyl glycine. Their 3D structures were in '.pdf' format in PubChem (Table S1, ESI†). Furthermore, 'pdbqt' files for the ligands were generated by Open Babel, followed by Grid Generation and Docking Analysis. Following the preparation of ligands and proteins, the molecular docking was conducted using Autodock (4.2.6 software). A grid with dimensions less than 1 Å specific to *X*, *Y*, and *Z* coordinates was established to encompass the protein, as done in the case of blind docking. This grid was centred around the protein to facilitate the most feasible docking conformations. Subsequently, the grid file was saved as a (.gpf) file. Then autogrid was initiated. Then, docking calculations were performed using the Lamarckian genetic algorithm (GA), fixing for 30 runs. The files were saved as a '.pdf'; final docking results were obtained after running the auto dock. dlg' file format showed H-bonding, binding energy and inhibition constants. The best docking conformations of the ligands with the receptors were selected based on the estimated binding energy (E_g) and inhibition constant (K_i). The protein–ligand complex with the lowest binding energy was extracted in the PDBQT format. Furthermore, the interactions between ligands and proteins of these complexes were extracted using LigPlot+, Autodock and ChimeraX in 2D and 3D.

2.6 Immunological studies

(a) Estimation of NF-κβ LEVEL. NF-κβ is an important group of proteins that regulates various cellular functions and inflammatory responses, and its deregulated activation contributes to the pathogenesis of various inflammatory diseases.[28] To check the immune responses of GlyNPs, it is crucial to check NF-κβ levels. In brief: RAW 264.7 macrophages (1×10^5 number of cells per well) were seeded in each well of a 96-well plate (A) and cultured in complete media for 24 h (at 37 °C, with 5% CO_2). Then, 0.2 μg mL^{-1} of LPS was added to each well and incubated for another 24 h to induce inflammation. Subsequently, GlyNPs were added to each well (with different doses such as 10, 20, 40, 100 and 150 μg mL^{-1}) and incubated for another 24 h. After 24 h, the 96-well plate was centrifuged at 960 rpm at 25 °C for 5 min to pellet debris. From each well of plate A, 20 μL of the culture supernatant was transferred into a new 96-well plate (B). Subsequently, 180 μL of the QUANTI-Blue assay solution was added (initially pink), followed by incubation at 37 °C for 1 h (the solution was turned purple). Then, the extent of SEAP expression level was calculated by measuring the intensity of the solution using a spectrophotometer (SPARK, TECAN, Männedorf, Switzerland) at 630 nm.

(b) Estimation of the level of NO generation. The anti-inflammatory property of the GlyNPs was estimated by measuring the extent of NO (nitric oxide) produced using LPS-treated RAW 264.7 macrophages. The lifetime of NO is very short in

water since it converts rapidly from NO to nitrite. The extent of NO produced was estimated for RAW 264.7 macrophages using the Griess reagent. First, RAW264.7 cells (1×10^5 cells/200 μL) were cultured in a 96-well plate and incubated in a CO_2 incubator for 24 hours with a continuous supply of 5% CO_2. Then, the cells were treated with LPS (0.2 μg mL^{-1} per well) to induce inflammation of the cells. The different extents of GlyNPs were added, and the treatment was followed for 24 h. Then, 100 μL of supplement was collected from each cell culture well, and 100 μL Griess reagent was added to each plate. Then, the generation of NO was quantified by measuring the absorption at λ_{max} = 550 nm using a microplate reader (Synergy H1, Biotech).

(c) Semi-quantitative real-time PCR (qRT-PCR) to estimate gene expression level. Semi-quantitative RT-PCR experiments were performed to determine the relative expression of genes that were finalised using network pharmacology. The main inflammation-related genes, such as TNF-α, IFN-γ, IL-6 and IL-10 with GAPDH as a control, were used as housekeeping genes. RAW 264.7 cells were seeded in 12 healthy plates and, other than control wells, treated with 100 μg mL^{-1} of GlyNPs after being stimulated with LPS (0.2 μg mL^{-1}). After 24 h, cells treated with GlyNPs were used for mRNA isolation. The total mRNA content was isolated using TRIZOL following the manufacturer's guidelines (Thermofisher). The RNA was quantified by spectrophotometer. Furthermore, the cDNA was prepared from RNA using a kit-based method (Thermo Fisher Scientific, RevertAid H Minus First Strand cDNA Synthesis Kit). The reverse transcription conditions were 95.0 °C for 2 min. For RT enzyme activation, it was kept at 95.0 °C for 10 s. The denaturation and melting were performed at 65.0–95.0 °C with 0.5 °C min^{-1} heating rate. The process was continued 39 times, and the melting curve was acquired within 65.0 °C to 95.0 °C (with 0.5 °C per 5 s heating rate). Briefly, 2 μL of cDNA (100 ng μL^{-1}), 1 μL of sense and antisense primer solutions (0.4 mM), 12.5 μL of SYBR Premix Ex Taq master mix (Takara Bio Inc.), and 9.5 μL of nuclease-free H_2O were mixed to obtain a final 25 μL reaction mixture in each reaction tube. A list of primer sequences for RT-PCR that are mentioned in Table 1 was taken for each specific gene. The gene-specific primers were amplified using a thermal cycler (Bio-Rad, Base Serial No.: CT058999 Optical Head Serial No.: 785BR31742).

2.7 Animal model of pristane-induced RA

In vivo studies were performed according to the Institute Animal Ethical Committee guidelines. A pristane-induced RA model was developed for the study.[29] A total of 9 Wistar rats each of weight 185 ± 5 gm were selected by a randomization method for the experiment. All animals were acclimated to the standard animal house environment for 7 days before initiation of the experiments. After the acclimatization, the animals were randomized into three groups based on body weight in individual cages. Herein, three groups of rats were employed. The first group of rats were treated with saline and referred to as the sham group. The second and third groups of rats were administered with 100 μL pristane (MP Biomedicals) through intradermal injection in each paw to induce arthritis. The rats of the second group were kept without treatment, and the rats of the third group were referred to as the treatment group. GlyNPs treatment was performed after full arthritis induction, which took 15 days to develop. The results obtained from the treatment group of rats were compared with the sham and positive control groups. The GlyNPs dose was decided as 2 mg kg^{-1} of rat (effectively 360 ± 10 μg GlyNPs) against inflammation (RA).

(a) Study the morphological changes: ankle and paw thickness. Since the start date of the experiment, the morphological changes of the paws of rats were measured to distinguish the onset of arthritic morphology. Ankle and paw thicknesses were measured with the help of a Vernier calliper with a periodical time period. Ankle thickness is a major phenotypic indication of RA. In RA, ankle thickness increases due to inflammation and an increase/decrease in ankle thickness was measured every two days. The results were compared with the sham and positive control groups of rats.

(b) Autoimmune and inflammatory marker panel. To check the levels of autoimmune and inflammatory markers at specific time periods, such as day 0, day 15, and day 30, the blood samples were collected from each rat group. To confirm the arthritis induction, the RA factors were checked by turbidimetric immunoassay (Turbilyte RF). The C-reactive protein (CRP) level was measured following the Immunoturbidimetry method (CRP Turbilatex) as per the manufacturer's protocol. Anti-double standard (dsDNA IgG ELISA, SKU DD037G), antinuclear antibody (ANA) (ANA Screen ELISA, SKU: AN033G) and anti-cyclic citrullinated peptide (anti-CCP) (anti CP IgG ELISA Kit, diametra, DK0149) levels were also measured according to the manufacturer's instructions. Uric acid levels were measured through the colourimetric test (Beckman AU480). Inflammatory parameters such as TNF-α, IL-1β and IL-6 in healthy and GlyNP-treated rats were checked by the ELISA kit method as per the manufacturer's protocol, before (on the 15th day of RA) and after the 30th day (15 days of post-treatment). The results were compared with the sham control and positive control groups.

Biosafety/ethical permission. All the *in vivo* studies were conducted according to the Institutional Animal Ethical Committee (IAEC) of Indian Institute of Technology (IIT), Banaras Hindu University, Varanasi guidelines (Registration no. 2123/GO/Re/S/21/CPCSEA) and approval (IAEC Approval No. IIT(BHU)/IAEC/2024/II/028, dated 13/09/2024).

Statistical analysis. The statistical analyses used Origin 2021, Student's *t*-test and one-way ANOVA. The data have been presented as mean ± standard deviation (S.D.). Statistical significance was calculated at a *p*-value of 0.05. Data was marked with '*' for $p < 0.05$, '**' for $p < 0.01$ and '***' for $p < 0.001$.

3. Results

Synthesis and characterization of glycine monomer and polymeric nanocapsules

As mentioned in the Method section, the GlyNPs have been synthesized. In the first step, glycine and acryloyl chloride were

synthesized by mini emulsion polymerization, followed by a modified method to the desired structure of the GlyNPs.[25,30] In the emulsion method, SDS, hexadecane, AIBN, and DVB are used as stabilizers, co-stabilizers of the emulsion, free radical initiators, and cross-linking agents, respectively. SDS and hexadecane were used to prevent the coalescence of the droplets and GlyNPs.

The chemical functionalities of the 'mers' and polymer particles were characterized through ^{1}H-NMR, ^{13}C-NMR (400 MHz, and solvent DMSO-d_6) and FTIR. The characteristic bands for glycine monomers are assigned as follows. ^{1}H-NMR (δ) (Fig S1, ESI†): 8.37 ppm (sec. amide), 6.29 ppm (*gem*, –C(═O) N), 6.07 ppm (*cis*, –C(═O)N), 6.13 ppm (*trans*, –C(═O)N), 3.45 ppm (2H, d); ^{13}C NMR (δ) (Fig. S2, ESI†): 171.66 ppm (–COOH), 165.79 ppm (amide –CO), 131.54 ppm, 131.31 ppm and 126.66 ppm (alkane adjacent to amide), and 41.37–39.05 ppm (aliphatic –CH). As shown in Fig. S1 and S2 (ESI†), the distinct bands assigned for glycine polymer are as follows. ^{1}H-NMR (δ) (Fig. S3, ESI†): 8.21 ppm (amide, 1H), 4.12–4.00 ppm (–CH_2 adjacent to amide) and 3.92–2.47 ppm (alkane –CH); ^{13}C NMR (δ) (Fig. S4, ESI†): (40.04–39.04 ppm) splitting of 2° alkane. For the glycine monomer, the characteristic FTIR bands obtained are at 3342 cm^{-1} for the secondary amine (–NH–) and overlapping broadband for hydroxyl (–OH), 2930 cm^{-1} for aliphatic stretching (–CH–), 2535 cm^{-1} for the carbon–carbon double bond in conjugation with carbonyl (═C–CO–), 1719 cm^{-1} for the carbonyl (–CO) group attached with a hydroxyl group, 1541 cm^{-1} for the (–CN–) amide band, 1450 cm^{-1} for the carbon–hydrogen aliphatic band (–C–H), and 1280 cm^{-1} for the amide band (–CN–). GlyNPs show characteristic bands at 3342 cm^{-1} for secondary amine (–NH–) and (–OH), 2930 cm^{-1} for aliphatic alkane stretching (–CH–, –CH_2), 1701 cm^{-1} for the carbonyl of the acid (–COOH) and 1602 cm^{-1} for the amide group (–CN) (Fig. 1(a)).

The morphology and particle size of the polymer particles were studied through HRTEM (Fig. 1(b) and (c)) and AFM (Fig. 1(f) and (g)). HRTEM results confirm that the sizes of the GlyNPs are in the range of 180–280 nm in diameter (Fig. 1(d)). Most of the particles are spherical in nature and many of them are core–shell in nature. The light core and darker shell structure are also observed for the hollow core–shell structure of the polymer particles with a core size of 150 ± 5 nm in diameter and a shell thickness of 65 ± 5 nm (Fig. S5, ESI†). It is also observed that the particles are porous in nature. The white spots highlighted with red circles of the particles are pores (HRTEM image, Fig. 1(c)). The average pore diameter is calculated to be 4–5 nm (Fig. 1(e)). Furthermore, to confirm the morphology of the particles, non-contact mode AFM was conducted and the particle sizes were measured from topographic 2D images and 3D images, and the particle size is calculated to be 137–150 nm in diameter (Fig. 1(f) and (g)), which is matching well with the results obtained from HRTEM. Thus, both the microscopy results revealed that the particles are monodispersed in nature. The monodispersed nature of the

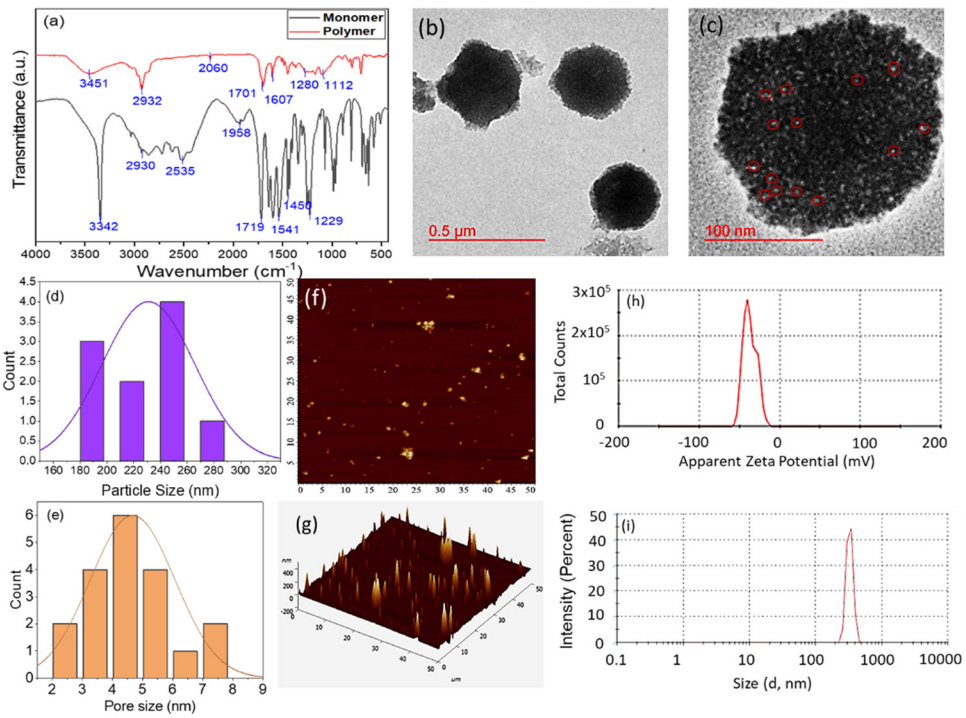

Fig. 1 (a) FTIR spectra showing the absorption band for the Gly monomers and polymers, (b) and (c) HRTEM images of GlyNPs at 0.5 µm and at 100 nm scale; (d) particle size distribution calculated from HRTEM images taking 100 particles, (e) pore size distribution of the particles calculated from (c), (f) AFM topography 2D image and (g) 3D AFM image; (h) plot for zeta potential results obtained from DLS and (i) hydrodynamic diameter of the polymeric particles calculated from a Zetasizer. Particles are of size 180–20 nm. The pore size obtained to be avg. 4–5 nm in diameter (highlighted with a red circle). (c) Zeta potential obtained to be −35.6 mV. Scale for the AFM image is in µm.

particles was also confirmed through DLS (particle size ~324 nm) (with PDI ~1.0) (Fig. 1(i)). This larger particle size value from DLS is obtained due to the hydrodynamic diameter. To confirm the colloidal stability of the polymeric particles, the zeta potential (ζ) was measured, and the value obtained was −35.6 mV, comprising the high colloidal stability of the polymeric particles (Fig. 1(h)).

Cell viability

The cell viability of the nanoparticles is crucial for their safe therapeutic applications. Polymeric nanoparticles have unique physicochemical properties that can lead to varying degrees of cytotoxicity depending on their size, shape, and surface chemistry. Therefore, the cell viability of the nanoparticles on RAW 264.7 macrophages (Fig. 2(a)) and PC-12 (Fig. 2(b)) is performed using an MTT assay, as mentioned in the Method section. RAW 264.7 cells, a murine macrophage cell line, are a useful model for evaluating the interaction of nanoparticles with immune cells. For inflammation and immunity, RAW 264.7 is the primary cell line for understanding the cytotoxic effects, and it can provide valuable insights into the biocompatibility and safety of NPs.[31] To support the cell friendliness, viability was further checked on PC-12 cells, and it is a widely used model cell line for studying the effects of nanoparticles on neuronal cells.[31] It is observed that with increasing the concentration from 10 μg mL^{-1} to higher, the cell viability for both RAW 264.7 and PC-12 cells varied. Cells are viable even at 100 μg mL^{-1} concentration of GlyNPs. We can assume that after 24 h of treatment, the % of viability varied due to experiencing contact inhibition by cells in the respective confined space. However, for both the cell lines, GlyNPs are taken in different concentrations such as 10, 20, 40, 80, 100, 125, 150, 200 and 250 μg mL^{-1}, and the % viability values relative to the control groups are found to be 91.4 ± 2.9, 90.9 ± 2.3, 86.2 ± 1.8, 87.4 ± 0.06, 79.6 ± 5.9, 80.2 ± 1.3, 71.4 ± 2.5, 66.01 ± 2.4 and 65.3 ± 4.8, respectively for RAW 264.7 macrophages. For PC-12 cells, the % viability varied from 136 ± 5.8, 134.72 ± 5.98, 119.38 ± 5.44, 111.57 ± 5.33, 90.09 ± 4, 88.71 ± 4.38, 85.97 ± 4.22, 82.52 ± 4.11, respectively. At lower concentrations, the observed higher viability of PC-12 cells compared to the control is attributed to a potential stimulatory or protective effect of the GlyNPs.

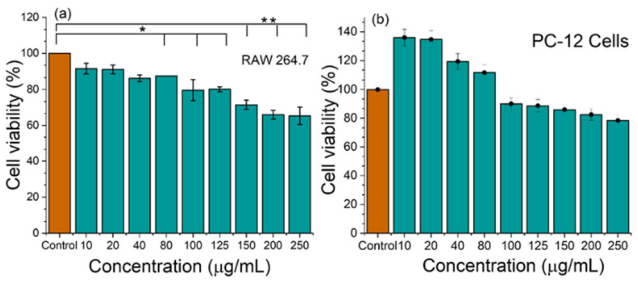

Fig. 2 The cell viability of GlyNPs with various concentrations. (a) Cell viability results on RAW 264.7 macrophages and (b) viability on the PC-12 cell line. Data was marked with '*' for $p < 0.05$, '**' for $p < 0.01$ and '***' for $p < 0.001$.

The GlyNPs at lower concentrations promote cellular activity, such as enhanced metabolic processes leading to increased viability as well as enhance the cell proliferation.

However, at higher concentrations of GlyNPs, the compound exceeds the threshold for such stimulatory effects and exhibits excellent cytotoxic effects. These results confirm that the Gly NPs are viable and suitable for therapeutic applications.

Cellular uptake of GlyNPs

The cellular uptake of NPs is a fundamental aspect of their functionality in therapeutic applications with target specificity. It influences the target efficiency of the therapeutic and safety profiles. To check the cellular uptake of GlyNPs, it was stained with Nile red and incubated with RAW 264.7 macrophages for 24 h with a non-toxic dose of 50 μg mL^{-1} followed by cell fixing and staining with DAPI to detect the nucleus. Then the confocal microscopy images of Nile red-GlyNPs were acquired (Fig. 3). The DAPI-stained cell nucleus was identified using the blue channel (λ_{exc} = 405 nm) (Fig. 3(a1)–(a3)) and fluorescence emission for the GlyNPs was observed using the red channel (λ_{exc} = 546 nm). The cellular uptake was qualitatively studied by acquiring fluorescence images after 24 h of incubation with Nile red-GlyNPs. From Fig. 3, it is clearly observed that GlyNPs were taken up inside the cell in the cytoplasm within 24 h of incubation. However, a considerable amount of uptake in the nucleus is less evident (Fig. S6, ESI†). This selective internalization suggested that the GlyNPs will further help to deliver biomolecules or drugs inside the cells. As GlyNPs are showing intracellular uptake, it is allowed to interact directly with the internal cellular machinery, which can be leveraged for therapeutic purposes. The uptake of GlyNPs by the immune cells (RAW 264.7) directs us to study their immune behaviour as they may change signalling pathways leading to the reduction of inflammation.

In silico study of GlyNPs

Network pharmacology. A network pharmacology study was performed to finalise the targeted genes that are responsible for RA following the steps mentioned in the Method section, and the results are shown in Fig. 4(a)–(c). From this study, we have confirmed the major targeted genes that are responsible for RA. From the GeneCards we have selected 6029 genes, from the MalaCards 313 genes and from DisGeNET we selected 2734 genes. With the help of Venny2.1.0, 218 common targets have been finalized, as shown in Fig. 4(a). The finalized common targets are considered in string tests for protein–protein interaction studies. The top 20 targets are taken for the network string interaction study, and they have been ranked according to the MCC method using Cytoskeleton software (Cytoscope3.10.2), and the results are shown in Fig. 4(b). The top 20 targets with their ranks are shown in Table S2 (ESI†), which included IFN-γ, IL-6, IL-10, IL1β, STAT-1, *etc.* targets for RA. In Fig. 4(b), the important targets are coloured according to the heat map. The red to yellow colour box of each target shows the intensity of higher to lower interaction. The string database provides a critical assessment and integration of protein–protein

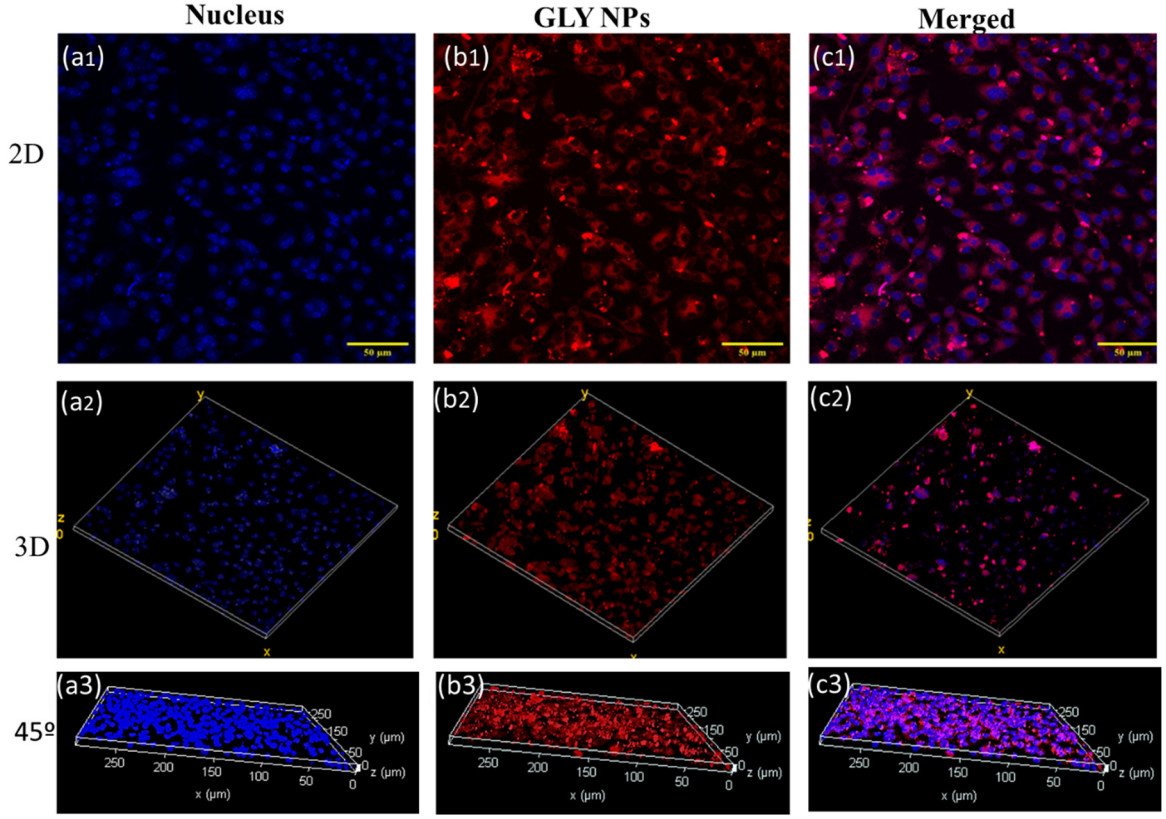

Fig. 3 The cellular uptake of GlyNPs, studied through confocal microscopy, (a1) 2D representation of the nucleus that is stained with DAPI, (a2) 3D representation of a1, (a3) 45° representation of cellular uptake where the *Z* axis shows the nucleus in 3D of the particles. (b1) 2D representation of GlyNPs stained with Nile red, (b2) 3D representation of b1, (b3) 45° representation of cellular uptake, where the *Z* axis shows internalisation of particles. (c1) 2D representation of GlyNPs stained with Nile red and the nucleus in blue colour, (c2) 3D representation of c1 and (c3) 45° representation of cellular uptake where the *Z* axis shows the internalisation of the particles.

interactions including direct interaction among the ranked targets (see Fig. 4(b)). Shiny Go results were used to finalize the targeted genes to determine the underlying molecular pathways and functional categories[32] as is shown in Fig. 4(c). These results revealed that the resulting genes are involved in various biological processes, including RA. These results further assured that the resulting genes are associated with the enrichment of RA up to 30 fold (Fig. 4(c)). Furthermore, from these targets, we have selected IL-6, IL-10, IL-1β, and STAT1 for further extensive docking, *in vitro*, and *in vivo* studies with other more prominent inflammatory markers, and the results are shown in the subsequent sections.

Molecular docking

Molecular docking is a critical computational technique for determining the ligand's optimal orientation and target protein after binding to form a stable complex. The knowledge of the binding modes has been utilized to calculate the binding affinity of the two molecules.[33] The docking approach has been utilized to rapidly screen vast databases of potential therapeutic compounds *in silico* to determine the favourable domains that are most likely to bind to proteins of interest.[34,35]

All the molecular docking studies were performed with specific inflammation-targeted protein receptors based on the network pharmacology analysis and previously reported anti-inflammatory activities. The blind docking results are obtained for all the inflammation-based targeted proteins such as COX2, NFκβ, IL-6, IL-1 β, TNF-α, iNOS, TLR-4, MAPK 14, MAPK 8, and STAT 1. For all the obtained results, the binding energy and interactions are shown in more detail in Tables S3–S12 (ESI†). Here, we have taken G1 (mer), G2 (dimer), G3 (trimer) and G4 (tetramer) of *N*-acryloyl glycine. We have used well-known anti-inflammatory drugs aspirin and diclofenac as controls.

For primary inflammatory receptor COX2 (pdb id 6COX), the binding energy values with aspirin and diclofenac are calculated to be −5.37 and −5.11 kcal mol^{-1}, respectively. Aspirin forms H-bonds with the HIS90 residue and diclofenac forms H-bonds with HIS90 and ARG513. Meanwhile, for G1, G2, G3, and G4, the binding energy values obtained were −5.17, −4.09, −3.39 and −3.54 kcal mol^{-1}, respectively. The H-bonds are majorly formed with G1 at ASN87, HIS90 and ARG513 residues, for G2 at HIS90 and TYR91, for G3 at HIS90, ASN87 and TYR91, and for G4 at HIS90 and TYR91 (see Table S3, ESI†). For primary inflammatory receptor NF-κβ, the binding energy values with aspirin and diclofenac are calculated to be −4.58 and −4.81 kcal mol^{-1}, respectively. Aspirin forms H-bonds with ARG54 and LYS241 residues and diclofenac forms H-bonds with LYS145 only. Whereas, for G1, G2, G3 and G4, the

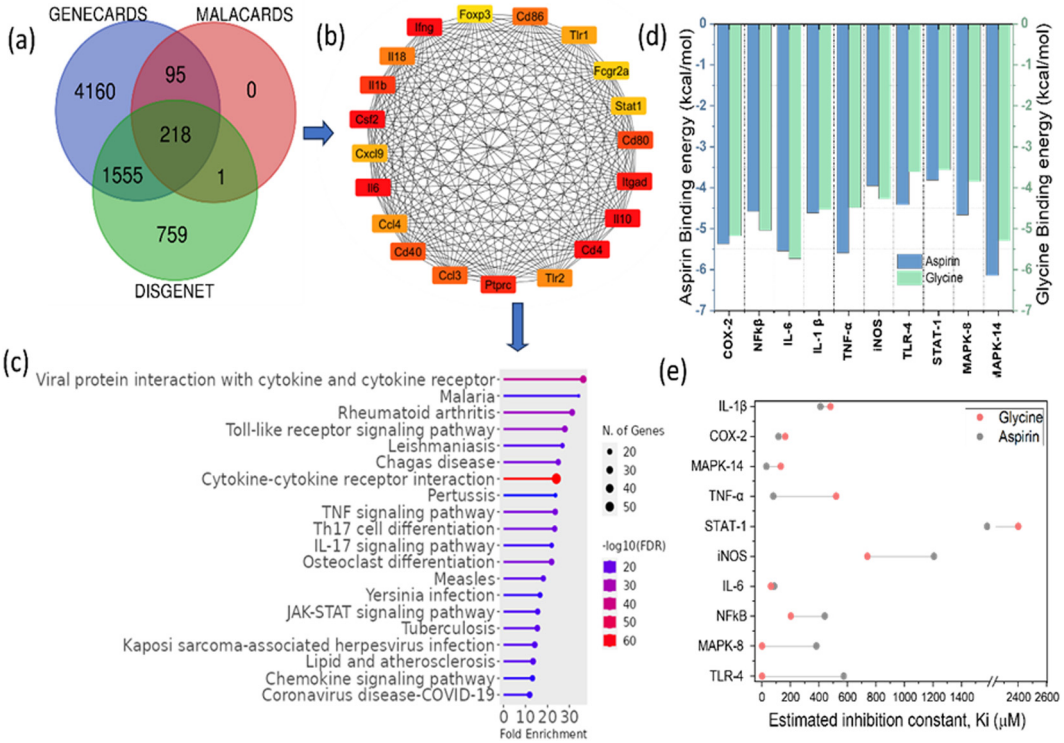

Fig. 4 Target network pharmacology and *in silico* investigation of GlyNPs. (a) Identification and prediction of common targeted genes and proteins utilizing three different databases represented by Venn diagram, (b) protein–protein interaction (PPI) network of the targeted proteins to understand the relationships between the targets (the red to yellow colour box of each target shows the intensity of higher to lower interaction) and (c) Shiny Go (lollipop) plot results obtained for the targeted genes involved in various biological processes including RA and their fold enrichment, (d) binding energy results obtained from the docking for different genes with glycine and aspirin associated to RA and inflammation, and (e) a comparison with the inhibition constant (K_i) of aspirin and GlyNPs in terms of estimation inhibition obtained from molecular docking for different target genes resulting from network pharmacology.

binding energy values were obtained to be −4.11, −5.04, −5.67 and −4.59 kcal mol^{-1}, respectively. The H-bonds are majorly formed with G1 at LYS114 and ASN136 residues, for G2 at LYS145 and LYS203, for G3 at LYS145 and LYS2023, and for G4 at LYS144 and LYS203 (see Table S4, ESI†).

For primary inflammatory receptor IL-6, the binding energy values with aspirin and diclofenac are calculated to be −5.54 and −6.74 kcal mol^{-1}, respectively. Aspirin forms H-bonds with LYS27 and ARG30 residues and diclofenac forms H-bonds with LYS27 only. Whereas, for G1, G2, G3 and G4, the binding energy values obtained were −4.88, −5.73, −4.55 and −4.80 kcal mol^{-1}, respectively. The H-bonds majorly formed with G1 at LYS27 and ARG30 residues similar to the control drug aspirin. For G2, the H-bonds majorly formed at ASP26 and LYS27 and ARG30, for G3 at LYS27 and ARG30, and for G4 at SER22, ASP26 and ARG182 (see Table S5, ESI†).

Similarly, it is found that IL-1β is also involved in the RA and inflammation. From the docking study, the binding energy values and the H-bond formation with different residues have been investigated and the results are shown in Table S6 (ESI†). The binding energy values with the aspirin and diclofenac are calculated to be −4.62 and −4.95 kcal mol^{-1}, respectively. Aspirin forms H-bonds with VAL3 and LYS93/94 residues and diclofenac forms H-bonds with LYS65 only. For G1, G2, G3 and G4, the binding energy values obtained were −4.53, −4.04, −3.07 and −2.10 kcal mol^{-1}, respectively. The H-bonds are majorly formed with G1 at ARG4, PHE46 and LYS93 residues. For G2, H-bonds prominently formed with ARG4, GLY49 and LYS93; for G3 with VAL3, GLN48 and LYS93; and for G4 at VAL3, GLN48 and LYS93/94 (see Table S6, ESI†). From these results, it is clearly evident that the obtained results are comparable to the aspirin and diclofenac.

The role of TNF-α in inflammation is well-known. The docking study has also been performed for TNF-α, and the results are shown in Table S6 (ESI†) in detail. The binding energy values with aspirin and diclofenac are calculated to be −5.59 and −4.89 kcal mol^{-1}, respectively. Aspirin forms H-bonds with VAL74 and LYS112 residues and diclofenac forms H-bonds with PRO70 and LYS112. For G1, G2, G3 and G4, the binding energy values were obtained to be −4.22, −4.48, −2.69 and −3.35 kcal mol^{-1}, respectively. The H-bonds majorly formed with G1 at PRO70 and LYS112 residues. For G2, the H-bonds majorly formed at LYS112 only, for G3 at CYS69, and for G4 at PRO70 and ARG103 (see Table S7, ESI†).

Inducible nitric oxide synthase (iNOS) is also a major mediator of inflammation. The docking study for iNOS was performed and the results are shown in Table S8 (ESI†) in detail. The binding energy values with aspirin and diclofenac

are calculated to be −3.95 and −4.42 kcal mol^{-1}, respectively. Aspirin forms H-bonds with HIS84 and diclofenac with the THR95 residue. For G1, G2, G3 and G4, the binding energy values were obtained to be −4.27, −6.00, −4.57 and −2.50 kcal mol^{-1}, respectively. The H-bonds predominantly formed with G1 at HIS84, for G2 at HIS 84 and ARG86, for G3 at ARG86 and LYS103, and for G4 at ARG86, THR95 and ARG452 (see Table S8, ESI†). Therefore, the HIS84 residue interacts with both the drugs and our GlyNPs.

Toll-like receptor (TLR4) possesses a central role in innate immune signalling and inflammatory responses by modulating the activity of transcription factors. A docking study has been performed and the results are shown in Table S9 (ESI†). The binding energy values with the aspirin and diclofenac are calculated to be −4.42 and −4.7 kcal mol^{-1}, respectively. Aspirin forms H-bonds with the LYS47 and ILE48 residues; for diclofenac, H-bonds formed only with LYS47. For G1, G2, G3 and G4, the binding energy values are calculated to be −3.88, −3.62, −3.26 and −2.74 kcal mol^{-1}, respectively. The H-bonds majorly formed for G1 at GLN281 and LYS254; for G2 at LYS229; for G3 at SER251 and LYS 282, and for G4 at LYS229/282 (see Table S9, ESI†).

Mitogen-activated protein kinase-14 (MAPK-14) (pdb id 4G1W) has an important role in the production of various pro-inflammatory cytokines and is an immune responsive component.[36] The docking results are shown in Table S10 (ESI†). The binding energy values with aspirin and diclofenac are calculated to be −6.14 and −6.95 kcal mol^{-1}, respectively. Aspirin forms H-bonds with LYS165 and diclofenac with the HIS126 residue. For G1, G2, G3 and G4, the binding energy values obtained were −4.56, −5.29, −4.44 and −4.64 kcal mol^{-1}, respectively. The H-bonds majorly formed for G1 at GLU160, G2 at HIS126, G3 at HIS126, and G4 at HIS126 sites (see Table S10, ESI†).

The final docking was performed with mitogen-activated protein kinase-8 (MAPK-8) (pdb id 4G1W), which is involved in the production of inflammatory cytokines. The docking results are shown in Table S11 (ESI†). The binding energy values with aspirin and diclofenac are calculated to be −4.66 and −4.12 kcal mol^{-1}, respectively. Aspirin forms H-bonds with LYS220 and diclofenac with LYS252. For G1, G2, G3 and G4, the binding energy values obtained are −3.85, −3.08, −2.85 and −2.49 kcal mol^{-1}, respectively. The H-bonds majorly formed with G1 at LYS203 and GLU204, and for G2, G3, and G4, H-bonds majorly formed with TYR202 and LYS203 residue sites (see Table S11, ESI†).

STAT1 is a key inflammatory gene responsible for inflammation as it is resulted from our network pharmacology analysis. The docking results are shown in Table S12 (ESI†). The binding energy values with the aspirin and diclofenac are calculated to be −3.82 and −3.6 kcal mol^{-1}, respectively. Aspirin forms H-bonds with TYR68 and diclofenac with ARG84. For G1, G2, G3 and G4, the binding energy values obtained are −3.33, −3.57, −2.36 and −1.16 kcal mol^{-1}, respectively. The H-bonds majorly formed with G1 at TYR106 and LYS110 residues. G2 has formed H-bonds majorly at LYS110/114, for G3 at LYS40 and ARG113, and for G4 at ARG113 sites (see Table S12, ESI†).

Furthermore, the binding interactions with GlyNPs (polymer, nanolattices) with 10 different selected targets are shown in the form of 2D and 3D images (Fig. 5). From 2D images, the residues in the hydrogen bonds are represented by green dotted lines and hydrophobic interactions highlighted with red semicircles (Fig. 5). 3D images show the overall groove available and pockets that interact with the ligands. This signalling activation leads to the onset of various inflammatory diseases.

Therefore, the network pharmacology results provided important information on the targets involved in the inflammation and the effective interactions of the polymeric particles synthesized in this work to reduce the inflammation. The binding residues and the inhibition constants (K_i) between G1, G2, G3, G4 and reference drug molecules with the targets are shown in (Tables S3–S12, ESI†) in detail.

Immunological responses of GlyNPs

Response of NF-κβ levels with GlyNPs. NF-κβ plays a central role in regulating inflammatory responses, and its dis-regulated activation contributes to the pathogenesis of various inflammatory diseases.[37] Furthermore, the NF-κβ is a key transcription factor that induces the expression of pro-inflammatory genes in both innate and adaptive immune cells.[28]

A colorimetric-based assay for detecting NF-κβ activation in macrophages was used to address this issue. The results are highlighted by activating the inflammation pathway with LPS since it is a well-known inflammation inducer. The LPS treatment upregulates NF-κβ concerning the control condition. The inflammatory modulation *via* the NF-κβ pathway has been compared by the response of macrophages, where other than the control, all the treatment groups are prepared for inflamed conditions with the help of LPS. The treatment condition is tested with different concentrations of GlyNPs, such as 10, 20, 40, 100, and 150 μg mL^{-1}. These concentrations were selected based on cell viability results obtained on macrophages, as shown in Fig. 2(a). The treatment with the GlyNPs shows suppression in inflammation with different concentrations (10, 20, 40, 100 and 150 μg mL^{-1}) and the values were calculated to be 1.72 ± 0.27, 1.70 ± 0.20, 1.32 ± 0.34, 1.15 ± 0.17 and 1.14 ± 0.14, respectively. It can be noted that, for the LPS-treated sample, the value of NF-κβ level obtained was 1.90 ± 0.07 (for 0.2 μg mL^{-1}), which is higher than the value obtained with GlyNPs. Therefore, in addition to NPs to LPS-treated cells, the NF-κβ levels varied, as shown in Fig. 6(a), and it is concentration dependent. These results indicated that the GlyNPs are an anti-inflammatory component (potential postbiotics). From Fig. 6(a), it is evident that the results represented here are statistically significant compared with the control for LPS, 10 μg mL^{-1} and 20 μg mL^{-1} of GlyNPs. To identify and confirm the underlying signalling pathways,[28] GlyNPs are used to reduce inflammation, so further study is required. However, a decrease in NF-κβ levels or activity would generally lead to reduced inflammatory responses by reducing the production of inflammatory mediators and generating inflammatory T cells. Furthermore, it modulates immune regulation by altering Treg cell development.[12]

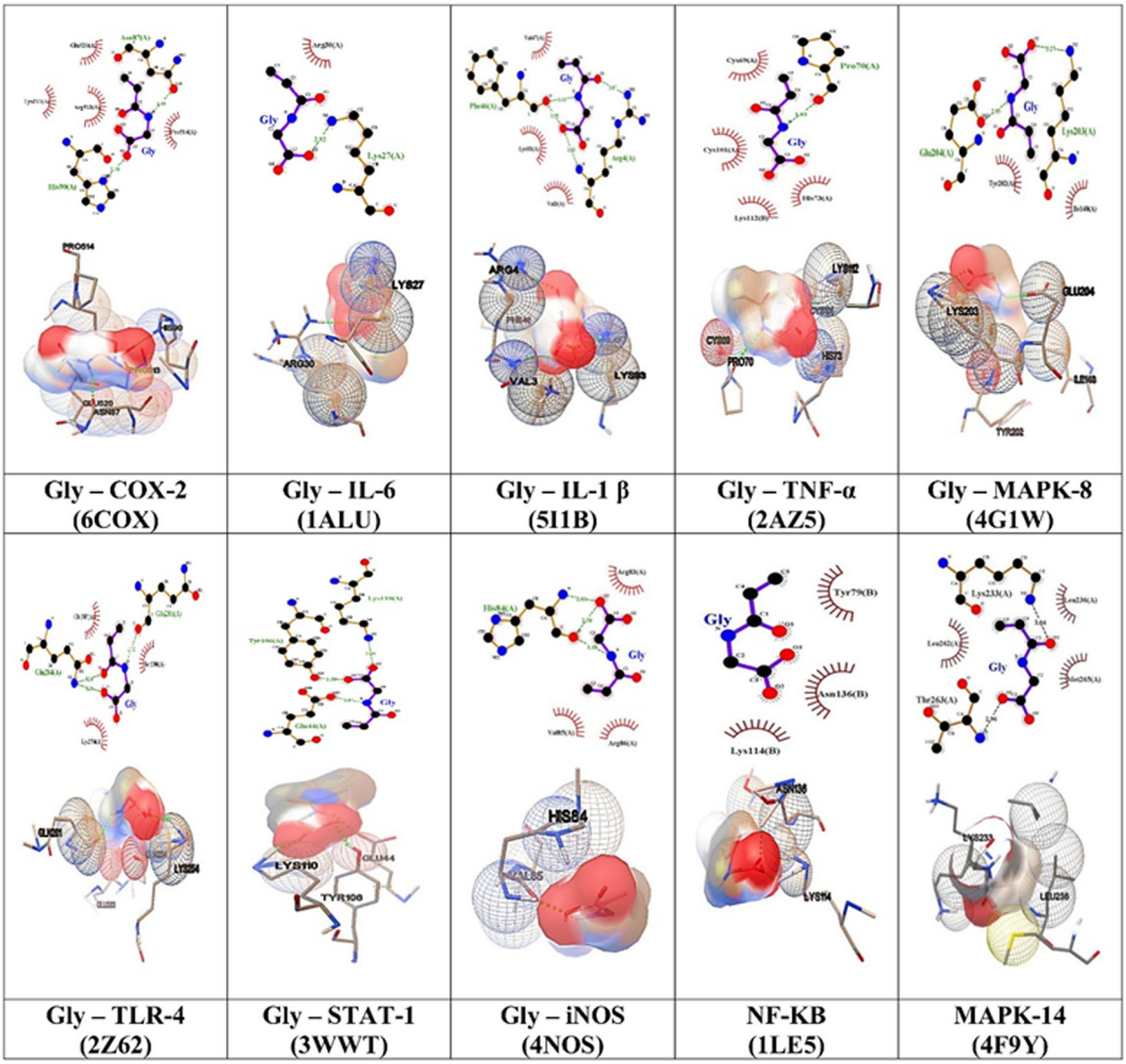

Fig. 5 *In silico* docking study to find out the molecular protein interactions with monomeric units of GlyNPs (G1). The interactions between polymer domain (G1) and molecular protein targets of COX2, NF-κβ, IL-6, IL-1 β, TNF-α, iNOS, TLR-4, MAPK 14, MAPK 8, and STAT1 responsible for the inflammation are presented. The binding interactions are depicted in 2D and 3D formats. Within the 2D images, the presence of residues engaged in hydrogen bonding is illustrated by green dotted lines, while hydrophobic interactions are emphasised with red hemi circles. 3D images comprehensively depict available grooves and pockets interacting with the ligands. The ligplots (2D images) showing the interactions between G1 (polymeric unit, monomer) with interacted residues along with binding energy in kcal mol^{-1} and inhibition constants (K_i). In the images, the red balls represent oxygen, the black balls represent carbon, and the blue balls represent nitrogen atoms.

NO production by GlyNPs

NO is a signalling molecule that plays a key role in the pathogenesis of inflammation and is involved in the generation of inflammatory disorders.[38,39] Therefore, NO inhibitors can be an important therapeutic option in managing inflammatory diseases.[40,41] To address the role of GlyNPs on NO production, macrophages (RAW 264.7 cells) were taken as model immune cells. Then, its anti-inflammatory effect under normal physiological conditions was determined with varying concentrations such as 10, 20, 40, 100 and 150 μg mL^{-1}. The production of NO by RAW 264.7 cells (taking 1×10^5 number of cells per well) was measured at λ_{max} = 540 nm (absorption band) with the help of Griess reagent, and the results are shown in Fig. 6(b). It is evident that with change in the doses of GlyNPs from 10, 20, 40, 100 and 150 μg mL^{-1}, the extent of NO release changes as 75.5%, 78.78%, 81.59%, 82.83% and 89.49%, respectively. The release of NO for the control sample (only cells) is considered 100%. Whereas, when the cells were treated with 0.2 μg mL^{-1} LPS using the same number of cells, the NO release enhanced to 104.83%. Thus, it is clearly evident that the rate of release of NO can be modulated with the extent of doses of GlyNPs used. Mechanistically, NO is produced in physiological conditions by nitric oxide synthase,[42] which converts into nitric oxide radicals ($NO^{\bullet}$) and can modulate inflammatory diseases such as RA. Therefore, controlling the NO production level with varying dosages of GlyNPs could be an alternate

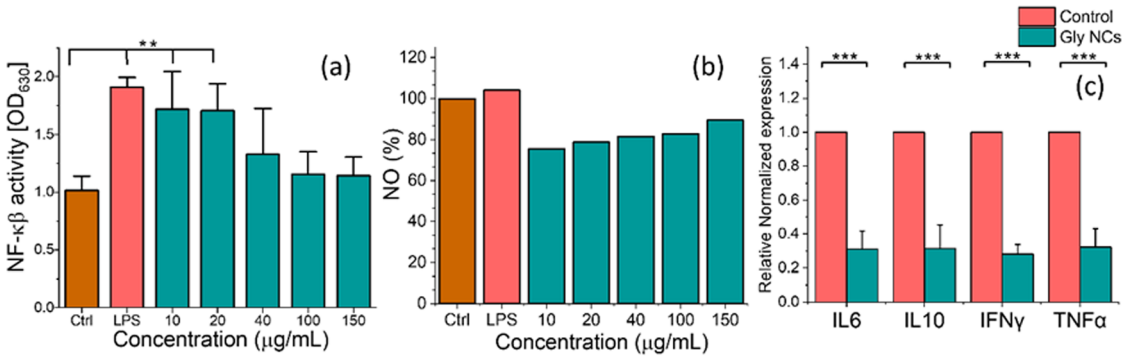

Fig. 6 *In vitro* immune response of GlyNPs and anti-inflammation behaviour studied for control cells, LPS-treated cells and cells treated with varying concentrations of GlyNPs, (a) NF-κβ level study, (b) NO release and response study, and (c) study of the response of inflammatory markers (TNF-α, IFN-γ, IL-6 and IL-10) and the results are compared with the control (only cells, 1×10^5 cells per well) and cells treated with LPS. The standard deviation and the significance of the results were estimated according to the procedure mentioned in the Method section (** for $p < 0.01$ and *** for $p < 0.001$).

strategy for treating inflammatory diseases such as rheumatoid arthritis (RA).

Response of the immunological markers

Inflammation is induced in cells, and GlyNPs were used with different concentrations (10, 20, 40, 100, and 150 μg mL^{-1}) to check their effectiveness. The suppression of NF-κβ and NO levels is noticed with the change in the concentration. Therefore, the effective dose is decided below 100 μg mL^{-1} for checking the status of the prominently involved immunological markers. Therefore, the inflammatory markers such as IL-6, IL-10, TNF-α and IFN-γ have been checked, and the results are shown in Fig. 6(c). RAW 264.7 cells (1×10^5 cells per well) were treated with a selected effective dose of GlyNPs (50 μg mL^{-1}) for 24 h. Then with the help of triazole, the RNA was isolated. RNA concentration was normalized with nuclease-free water for cDNA synthesis, and RT-PCR experiments were performed as mentioned in the Experimental section. The RT-PCR results are shown in Fig. 6(c), with the genetic expression of inflammatory markers for IL-6, IL-10, TNF-α and IFN-γ. IL-6 plays an essential role in cell signalling and acute inflammation, and it is required for the rapid resolution of wound healing. From Fig. 6(c), it is evident that the IL-6 level is decreased from the control to GlyNP-treated sample. According to the heat map gene expression results, there is a 3.237 fold reduction in IL-6, comprising a quite excellent anti-inflammatory effect of the GlyNPs. It is also noted that IL-10 is an anti-inflammatory cytokine. It maintains the equilibrium for the immune response, allowing the clearance of infections. Therefore, the IL-10 expression levels were also calculated using the same approach. From the relative normalized heat map gene expression results (Fig. 6(c)), it is clearly evident that there is a 3.377 fold reduction in IL-10 level, which comprises an excellent anti-inflammatory effect of the GlyNPs. It can also be noted that the IL-10 level possesses an M2-like macrophage phenotype that is strongly suggested for particles' (GlyNPs) anti-inflammatory properties.[43] Their values have been calculated under similar experimental conditions to confirm the normalised gene expression levels of TNF-α and IFN-γ. From Fig. 6(c), it is evident that the TNF-α level decreased from control to GlyNP-treated cells by 2.991 fold; for IFN-γ, it decreased by 3.469 fold. This reduction in the expression of these cytokines can lead to the conclusion that the GlyNPs are not only anti-inflammatory in nature, but can also play an essential role in modulating the host's innate immunity. Therefore, these findings are crucial in reducing inflammation by modulating immune response, such as in RA.[44] However, the ratio in the expression of these cytokine levels does not change significantly, showing a balanced reduction in the expression of the overall cytokines, and the results are statistically significant.

In vivo anti-inflammatory efficiency of GlyNPs on an RA model

Morphological changes: ankle and paw thickness with treatment period. The ankle thickness usually increases due to inflammation, a major phenotypic indication of the RA condition. RA was induced to determine the impact of the GlyNPs on inflammation, with the help of pristane according to the method mentioned in the Experimental section. The treatment has been performed and the results are shown in Fig. 7. The ankle and paw thickness (mm) of each rat was measured with a Vernier calliper on the 0th, 7th, 15th, 20th, 25th and 30th day. The total *in vivo* treatment period is shown in Fig. 7(a). After induction of pristane, it took 15 days to develop inflammation (RA), as shown in Fig. 7(b). The GlyNPs doses were induced on day 15 and day 22 for the treatment group of rats, whereas for sham and positive control groups of rats no treatment doses of GlyNPs were given. It is evident from Fig. 7(b) that in the sham control group of rats, the paw thickness varied from 3.01 ± 0.22 mm to 3.20 ± 0.20 from the 0th day to the 30th day. For the positive control group of rats (treated with pristane), the paw thickness (left leg) increased from 3.43 ± 0.30 mm (on the 0th day) to 5.55 ± 0.30 mm (on the 15th day), and finally, on the 30th day, it is calculated to be 5.32 ± 0.11 mm. Meanwhile, for the treatment group of rats, the paw thickness (left leg) changes from 5.37 ± 0.59 mm (inflammation state) to 4.20 ± 0.26 mm (inflammation reduced state). It can be noted that the paw thickness (left) for the treatment group of rats from the 0th day to the 15th and

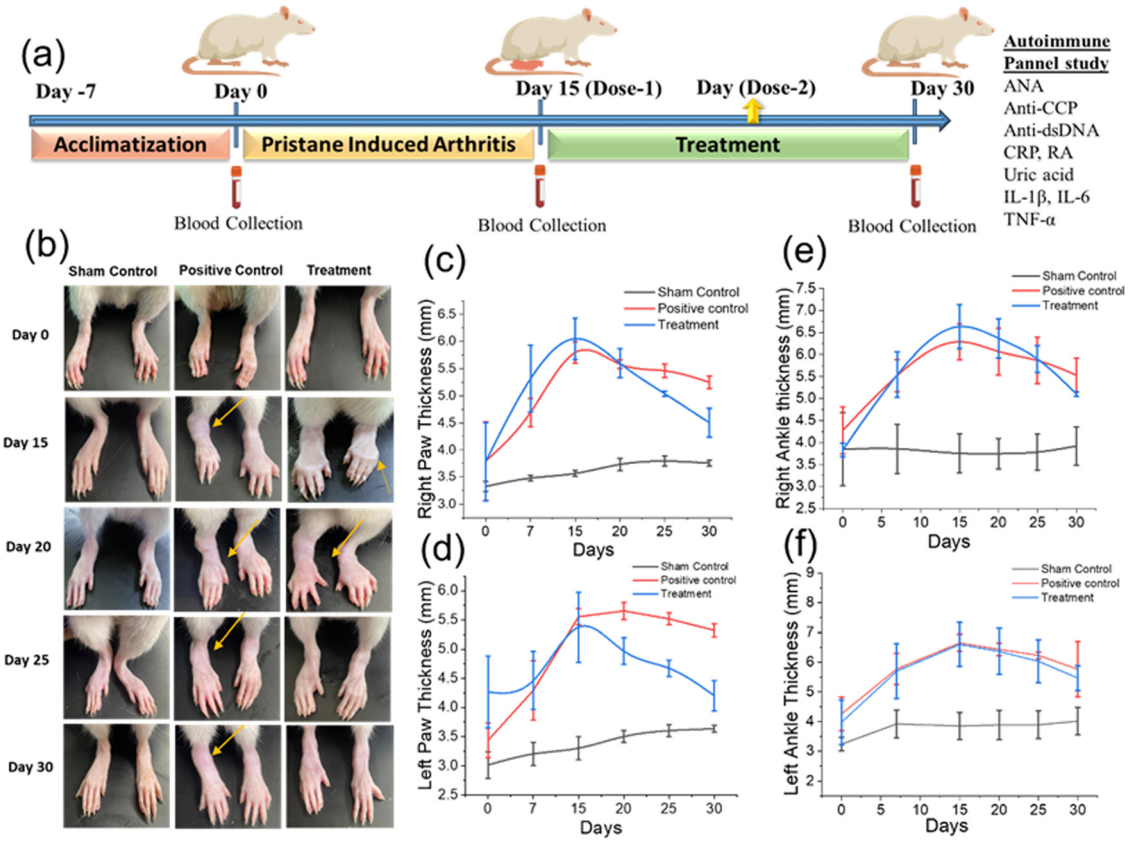

Fig. 7 The study of *in vivo* anti-inflammation (RA) potential of GlyNPs. (a) Schematic plan for the entire *in vivo* experimental and treatment plan followed by an autoimmune panel study plan. (b) Camera photographic images of the sham control, positive control and GlyNP-treated rats showing the morphological changes in paw oedema at different days to study the anti-inflammation effects. (c) and (d) The change in thickness of the right and left paws, respectively, of the rats on different days. (e) and (f) Change in thickness of the right and left ankles, respectively, of the rats on different days.

30th-day changes from 4.20 ± 0.61 mm to 5.37 ± 0.59 mm (inflammation state) and 4.20 ± 0.26 mm (inflammation reduced state), respectively. Thus, it is evident that the inflammation in paw thickness for the treatment group of rats is reduced by 95–99%. This means that the paw thickness has come back to its initial stage. Similarly, the right paw thickness for the treatment group of rats changed from 3.78 ± 0.72 (0th day) to 5.6 ± 0.24 mm (15th day, inflammation developed) and 4.50 ± 0.26 (after treatment on the 30th day), respectively, which represents a clear 80–90% reduction in inflammation after treatment. The detailed results are represented in Fig. 7(b)–(d). Similar types of results are also obtained when we studied the ankle thickness for the sham, positive control and treatment group of rats (see Fig. 7(b), (e) and (f)). Therefore, it can be concluded that the GlyNPs have an effective role in reducing inflammation (RA) at the phenotypic level. The camera photographs shown in Fig. 7(b) are clear evidences for the same.

Autoimmune and inflammatory marker panel

As mentioned earlier, with the development of inflammation (RA), various biochemical parameters associated with autoimmunity can be changed. Therefore, studying these parameters is crucial for sham, positive control and GlyNP-treated rats. Herein, we have studied the levels of the RA factor, anti-cyclic citrullinated peptide (anti-CCP), antinuclear antibody (ANA), anti-double stranded DNA antibodies (anti-dsDNA), CRP, and uric acid levels on different days of treatment and the results are shown in the subsequent sections (see Fig. 8(a)–(f)).

Rheumatoid factor (RF)

RF is an antibody made by our immune system and facilitates the formation of immune complexes, which contribute to the inflammatory characteristic of RA.[45] Therefore, it is very important to determine the RF levels of the rats used in the *in vivo* anti-inflammation study for this work. Hence, the blood serum samples were collected from GlyNP-treated, sham and positive control rats to perform the RF test on day 0 (before inducing pristane to develop RA), 15 (after RA developed and before treatment started) and 30 (after 15 days of post-treatment). Then, the RF values were calculated through the turbidimetric immunoassay on the above-specified days, and the results are shown in Fig. 8(a). The RF levels for all the sham control rats at day 0th, day 15th and day 30th are found to be 1.7 ± 0.26, 1.96 ± 0.20 and 2.03 ± 0.15 IU mL^{-1}, respectively. For the positive control group of rats, the RF levels are found to be 1.94 ± 0.19, 5.56 ± 0.25 and 4.03 ± 0.35 IU mL^{-1} on day 0, day 15 and day 30, respectively. Whereas, for the treatment

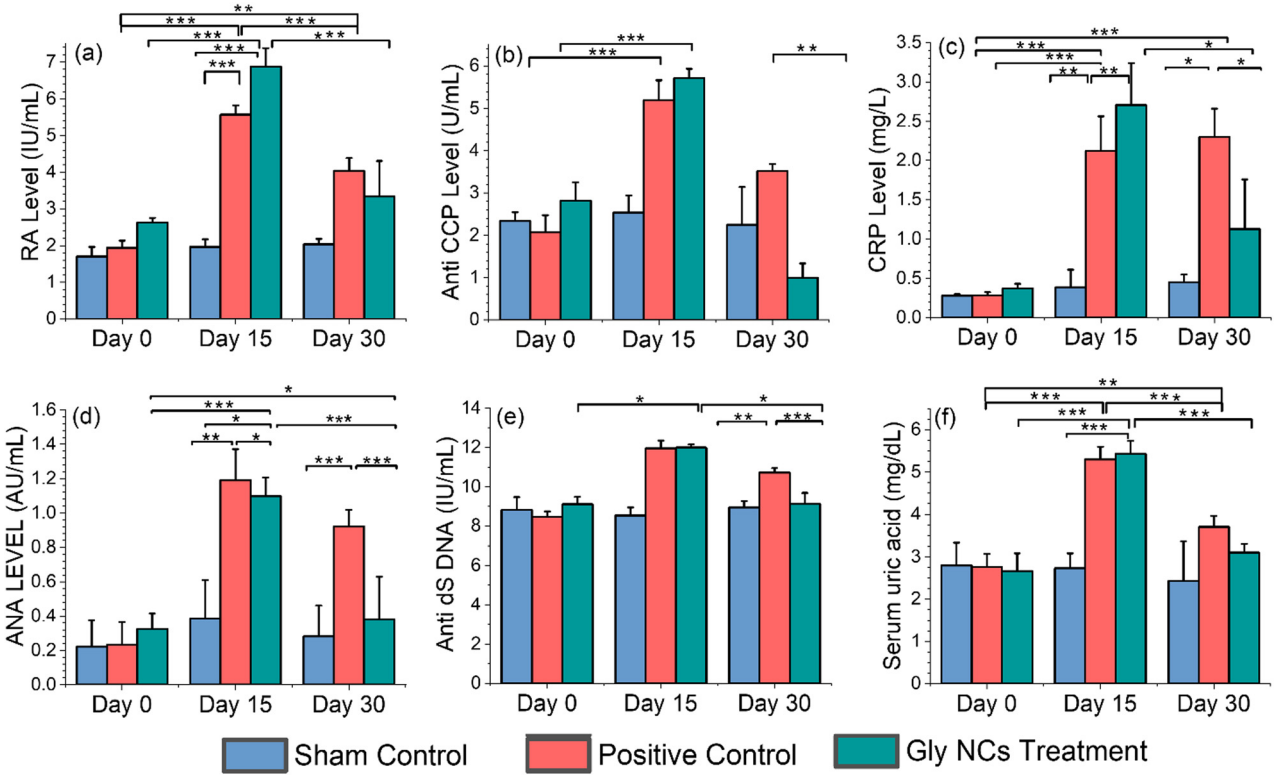

Fig. 8 Study of the autoimmune and inflammatory marker levels. (a) RA level, (b) anti-CCP, (c) CRP level, (d) ANA level, (e) anti-dsDNA and (f) serum uric acid levels obtained on day 0, 15 and 30. Statistical significance was calculated at a p-value of 0.05. Data was marked with '*' for $p < 0.05$, '**' for $p < 0.01$ and '***' for $p < 0.001$.

group of rats, the RF levels were calculated to be 2.1 ± 0.1 and 5.5 ± 0.4 IU mL^{-1} on day 0 (*i.e.* when no inflammation is there) and on day 15 (when inflammation was developed). However, after 15 days of post-treatment with GlyNPs (*i.e.*, on the 30th day), the RF level decreased to 2.66 ± 0.77 IU mL^{-1}. This RF level is almost in the order of the RF level of the sham control group of rats. Therefore, the effectiveness of GlyNPs at the onsite delivery shows wonderful results for the reduction of inflammation and RA. Furthermore, the clinical significance of the RF levels has been studied by the other diagnostic tests that have been reported in the subsequent sections. However, the reduction in the RF level for the positive control rats (rats with RA developed but not treated with GlyNPs) from 5.56 ± 0.25 and 4.03 ± 0.35 IU mL^{-1} for day 15 and day 30, respectively, signifies the autoimmune response of the body. In conclusion, GlyNPs are effective in reducing RF levels and inflammation.

Anti-cyclic citrullinated peptide (anti-CCP)

High anti-CCP levels are usually common in severe RA. Furthermore, the increase in anti-CCP level is directly proportional to the tissue and joint damage. Therefore, the detection of anti-CCP levels is essential to determine the severity of inflammation as well as RA. Hence, the blood serum levels were collected from all the rats under experiments to perform the anti-CCP test on day 0 (before inducing pristane), 15 (after RA developed and before the treatment started) and 30 (15 days post-treatment). Then, the anti-CCP levels were calculated using the ELISA kit on the above-specified days, and the results are shown in Fig. 8(b).

The anti-CCP levels for all the sham control rats at day 0, day 15 and day 30 are found to be 2.33 ± 0.20 AU mL^{-1}, 2.53 ± 0.40 AU mL^{-1} and 2.24 ± 0.89 AU mL^{-1}, respectively. For the positive control group of rats, the anti-CCP levels were found to be 2.06 ± 0.40, 5.19 ± 0.469 and 3.51 ± 0.17 IU mL^{-1} on day 0, day 15 and day 30, respectively. Whereas, for the treatment group of rats the anti-CCP levels were calculated to be 2.06 ± 0.40 and 5.19 ± 0.469 IU mL^{-1} on day 0 (*i.e.*, when no inflammation is there) and day 15 (when inflammation was developed), respectively and after 15 days without GlyNP treatment (*i.e.*, on 30th day), the anti-CCP level is decreased to 3.51 ± 0.17 IU mL^{-1}, indicating the decrease in the severity of RA due to autoimmunity. However, after 15 days of post-treatment with GlyNPs (*i.e.*, on the 30th day), the anti-CCP level decreased to 0.920 ± 0.31 IU mL^{-1}. This reduction in the anti-CCP level gives strong evidence for the anti-inflammatory activity of GlyNPs.

Effect of GlyNPs on CRP levels

CRP is an acute-phase reactant pentameric protein synthesized by the liver and is directly related to the inflammation induced by IL-6. It plays a crucial role in the body's immune system by binding to pathogens and damaging cells.[46] In RA, CRP serves as a biomarker for analysing its severity. The increase in CRP levels can increase joint inflammation and damage the

tissues.[47] Therefore, the detection of CRP levels is essential to find out the severity of inflammation as well as RA. To measure the CRP levels, the blood serum samples from all the rats under experiments were collected on day 0 (before inducing pristane), 15 (after RA developed and before the treatment started) and 30 (15 days post-treatment). The CRP levels were calculated using the ELISA kit, as mentioned earlier, and the results are shown in Fig. 8(c). It is clearly evident that for the sham control group of rats, the CRP level changes from 0.28 ± 0.02 to 0.38 ± 0.22 and 0.45 ± 0.1 mg L^{-1} from day 0 to 15 and 30, respectively. For the positive control group, the CRP level changes from 0.26 ± 0.041 mg L^{-1} (on day 0th) to 1.93 ± 0.37 mg L^{-1} (on day 15th), that is, after pristane injection (RA development). Further, it is noticed that for the positive control group of rats, the CRP level reached 2.3 ± 0.3 mg L^{-1} on the 30th day, demonstrating the increase in severity of inflammation of RA. Interestingly, after 15 days of immunization (post-treatment) with GlyNPs, the CRP level for the treatment group of rats came down from 1.99 ± 0.37 mg L^{-1} (from severe inflammation state, day 15 of RA) to 0.80 ± 0.45 mg L^{-1}, which comprises strong evidence for the anti-inflammatory and anti-RA potential of GlyNPs.

Antinuclear antibody (ANA) levels

Antinuclear antibody (ANA) testing is an important screening tool for autoimmune conditions. ANA binds DNA or associated nucleosome proteins.[48] ANA correlates with elevated C-reactive protein (CRP) levels and increased joint inflammation in RA patients. Recent research highlights that ANA-positive patients with RA have different clinical characteristics than their ANA-negative patients. Significantly, a positive ANA level is associated with RA, which can be reduced with anti-rheumatic drugs.[49] Hence, ANA levels were checked with the help of an ELISA test on day 0, day 15 (inflammation achieved), and day 30 (treatment), and the results are shown in Fig. 8(d).

It is clearly evident that for all three groups of rats, the ANA levels range between 0.22 ± 0.15 AU mL^{-1} to 0.32 ± 0.09 AU mL^{-1} on day 0. On day 15, the ANA levels for the sham, positive control and treatment group of rats were found to be 0.38 ± 0.22 AU mL^{-1}, 1.19 ± 0.18 AU mL^{-1} and 1.09 ± 0.10 AU mL^{-1}, respectively. On day 30, the ANF levels for the sham, positive control and treatment group of rats are found to be 0.28 ± 0.17 AU mL^{-1}, 0.92 ± 0.08 AU mL^{-1} and 0.37 ± 0.024 AU mL^{-1}, respectively. Therefore, on treatment with GlyNPs, the ANA level decreased approximately to a similar value as on day 0. Whereas for the positive control, in the RA developed rat group, it reduced only by $\sim$20%, possibly due to the natural immune response. Thus, it can be concluded that the GlyNPs impact the reduction of the ANA levels as well as the inflammation due to RA.

Anti-double-stranded DNA antibodies (anti-dsDNA)

Anti-dsDNA is an antibody that targets double-stranded DNA molecules in the nucleus of cells in the human body and is one of the important antibodies for autoimmune disorders.[50] Therefore, checking the anti-dsDNA antibody levels for RA patients is very important. Various studies have reported that 82.92% of RA patients tested positive for anti-dsDNA antibodies.[51] Furthermore, anti-dsDNA antibodies can be generated by anti-TNFα, which modulates inflammation status.[52] Hence, anti-dsDNA levels were checked with the help of an ELISA test on day 0, day 15 (inflammation achieved), and day 30 (treatment), and the results are shown in Fig. 8(e). It is clearly evident that the anti-dsDNA levels for days 0, 15 and 30 are found to be 8.81 ± 0.65 IU mL^{-1}, 8.53 ± 0.40 IU mL^{-1} and 8.93 ± 0.33 IU mL^{-1} for sham control, *i.e.*, there is no change in the values. The positive control rats' value changed from 11.95 ± 0.38 IU mL^{-1} (15th day) to 10.71 ± 0.22 IU mL^{-1} for the 30th day (no treatment performed). However, for the treatment group of rats, the anti-dsDNA level changes from 11.13 ± 0.14 IU mL^{-1} (15th day) to 8.46 ± 0.52 IU mL^{-1} for the 30th day (on treatment with GlyNPs). This value is equal to the anti-dsDNA level of the 0th day. Thus, this result is strong evidence that GlyNPs effectively reduce inflammation.

Study of the uric acid levels

Uric acid is the final waste product of purine metabolism, and it can lead to gout and kidney stones and potentially affect joint health due to crystal formation in the joints.[53] Increasing uric acid levels contribute to inflammation, joint damage, and RA. Hence, the uric acid levels were checked on day 0, day 15 (inflammation achieved), and day 30 (treatment), and the results are shown in Fig. 8(f). The uric acid levels for all the sham control rats at day 0, day 15 and day 30 are found to be 2.8 ± 0.52, 2.73 ± 0.35 and 2.43 ± 0.92 mg dL^{-1}, respectively. For the positive control group of rats, the uric acid levels are calculated to be 2.76 ± 0.30, 5.30 ± 0.3 and 3.7 ± 0.26 mg dL^{-1} on day 0, day 15 and day 30, respectively. Whereas, for the treatment group of rats, the uric acid levels were calculated to be 2.66 ± 0.41, 5.43 ± 0.30, 3.1 ± 0.20 mg dL^{-1} on day 0 (*i.e.*, when no inflammation is there) and day 15 (when inflammation was developed), and on day 30 (means 15 days after post-treatment), respectively. Therefore, after 15 days post-treatment with GlyNPs (*i.e.*, on the 30th day), the uric acid level decreased almost to the level of day 0. In conclusion, this radical change in the uric acid level makes strong evidence for the anti-inflammatory and anti-RA activity of GlyNPs.

Inflammatory parameter in rats

IL-1β is a potent pro-inflammatory cytokine, and it is crucial for host defence against infection and injuries[54] IL-1β also serves an important role in the pathogenesis of inflammation and RA.[55,56]

TNF-α is a potent pro-inflammatory cytokine that modulates facets of macrophage functions, and it is rapidly released after trauma and chronic infections. It has been shown to be one of the most abundant early inflamed tissues.[57] Furthermore, it can potentially trigger pathological implications, including autoimmune illnesses.[58] Therefore, it is very important to determine the level of immune markers such as IL-1β, TNF-α and IL-6 in healthy sham, positive control and GlyNP-treated rats. To measure these parameters, the blood serum samples from all the groups of rats were collected, and experiments were

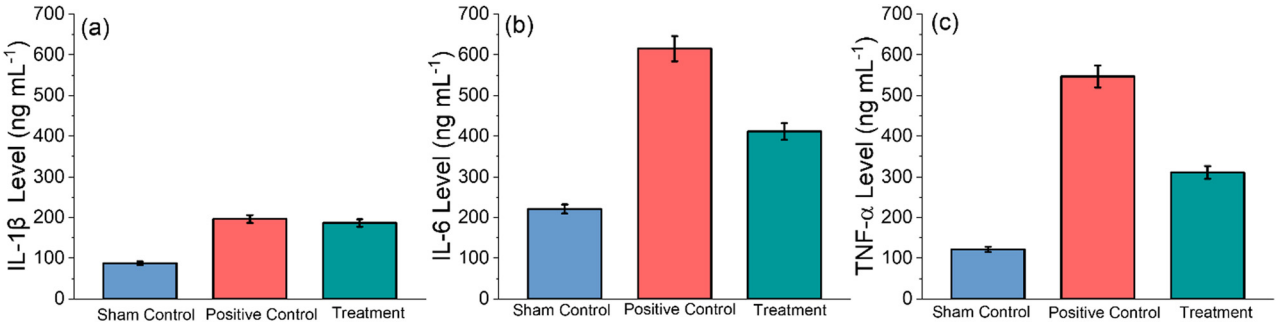

Fig. 9 Study of the *in vivo* immune cytokines to check the inflammatory parameters for the Sham, positive control and treatment group of rats: (a) IL-1β Level, (b) IL-6 and (c) TNF-α level. This study was performed on the 30th day, *i.e.*, after 15 days post-treatment.

performed through the ELISA kit, as mentioned in the Method section. The results are shown in Fig. 9(a)–(c). It can be noted that the IL-1β, TNF-α and IL-6 levels were measured on the 30th day, *i.e.*, 15 days post-treatment. It is evident from Fig. 9(a) that the IL-1β levels in the control sham, positive control and GlyNP treated group of rats are found to be 87.56 ± 4.37, 196.32 ± 9.81 and treatment 186.54 ± 9.32 ng L^{-1}, respectively. The IL-6 levels in the control sham, positive control and GlyNP-treated group of rats observed to be 221.10 ± 11.05, 615.42 ± 30.77 and treatment 411.46 ± 20.57 ng L^{-1}, respectively (Fig. 9(b)). The TNF-α levels, as shown in Fig. 9(c) for the sham control group, positive control and GlyNP-treated group of rats, are found to be 121.56 ± 6.07, 547.22 ± 27.36 and 311.20 ± 15.56 ng L^{-1}, respectively. Thus, from all these results, it can be concluded that the GlyNPs potentially reduce inflammation due to RA.

4. Discussion

Inflammatory diseases are very common nowadays due to various reasons[59,60] and patients suffer a lot, irrespective of age.[1] Severe inflammation causes RA, inflammatory bowel disease, psoriasis, and systemic lupus erythematosus.[2] The inflammation can cause tissue injury, organ dysfunction, and damage organs severely.[3,4] Therefore, there is an urgent need to develop new therapeutics and strategies to mitigate inflammatory diseases and improve patients' recovery outcomes from the existing treatment options. Extensive research works using inorganic nanoparticles, enzymes, nanobodies, PEGylates, *etc.*[16,17,61] have been conducted. However, over the past three decades, it has not gained remarkable advancements to cure inflammatory disorders. Hence, the present state-of-the-art work is very much promising in this challenging scenario.

In this work, we have developed porous GlyNPs of size 180–250 nm with pore size of 4–5 nm in diameter using glycine and acryloyl chloride (Fig. 1(a)–(g)). GlyNPs also exhibit colloidal stability (ζ = −35.6) (Fig. 1(h)). The advantage of these GlyNPs is that they are biocompatible in a broad concentration range (10–250 μg mL^{-1}) (tested on RAW 264.7 macrophages, immune cells, Fig. 2(a), and PC-12 cells, neuronal cells, Fig. 2(b)). GlyNPs are proliferative in nature at a low concentration, such as 80 μg mL^{-1} (Fig. 2(b)). Based on the proliferative nature, polymeric nanoparticles of glycine have been used earlier for wound healing and to reduce the inflammation of wounds only by our research group where the nanoparticles were of size below 50 nm.[25] At lower concentrations, the observed higher viability of PC-12 cells compared to the control is attributed to a potential stimulatory and protective effect of GlyNPs. The GlyNPs at lower concentrations promote cellular activity, such as enhanced metabolic processes leading to increased viability and enhanced cell proliferation (Fig. 2(b))[62] resembling its suitability for therapeutic applications. Usually, inorganic/metal NPs below a size of 8 nm in diameter can be easily excreted through the urinary tract.[63] Charged NPs can circulate in the blood for a longer period of time due to the coulombic interactions.[63] The advantages of using the amino acid polymeric nanoparticles are: (i) they are degradable in nature, and (ii) their degraded products are not toxic (as we have reported earlier for a similar type of polymer),[64] and (iii) the debris, which could be excreted easily through the urinary tract.

Different types of nanoparticles can be internalized into the cells (macrophages and endothelial cells) through various processes, such as receptor-mediated or caveolin-mediated endocytosis. The cellular internalization mechanisms strongly depend on the type of nanoparticles, their size and shapes, and surface properties.[65] However, the actual mechanisms of internalization of nanoparticles are still elusive. In this study, we have studied the cellular internalization of GlyNPs (Fig. 3) through confocal microscopy, since the internalization of these NPs regulates the secretion of inflammation-specific markers[66,67] such as IL-6, IL-1β, TNF-α, TLR-4, STAT-1, MAPK-8, MAPK-14, iNOS, NF-κβ and COX-2, that were identified from Network pharmacology and through the *in silico* study (Fig. 4 and 5). To validate the secretion of inflammation-specific markers, we have performed *in vitro* study on the macrophages by varying the concentrations of GlyNPs (Fig. 6) under a cell-based inflammation model. The cell-based inflammation was generated using LPS. The results show that the GlyNPs with different concentrations regulate the secretion levels of NO, NF-κβ, INF-γ, IL-6, IL-10, and TNF-α, comprising the reduction of inflammation (Fig. 6).

To validate the therapeutic efficiency of GlyNPs, an RA model has been developed with rats, and it is observed that controlling the levels of IL-1β, TNF-α and IL-6 within 15 days of

post-treatment can reduce the inflammation. The autoimmune and inflammatory markers such as (a) RA, (b) anti-CCP, (c) CRP, (d) ANA, (e) anti-dsDNA and (f) serum uric acid levels observed are reduced compared to the control and sham group of rats within 15 days post-treatment. The results obtained are at a statistically significant level (the statistical significance was calculated at a p-value of 0.05. Data was marked with '*' for $p < 0.05$, '**' for $p < 0.01$ and '***' for $p < 0.001$). Thus, GlyNPs provide excellent anti-inflammatory properties to reduce the impact of RA. It can be noted that complicated autoimmune diseases, such as RA, can cause severe articular damage (cardiovascular problem) and reduce the life quality of patients.[45,68] Using GlyNP treatment, the patient's life quality can be improved, for which extensive clinical research is required. A series of nanoparticles were used for the treatment of inflammatory bowel disease.[69,70] However, amino acid-based nanoparticles or GlyNPs have never been used, which may have better therapeutic efficiency. Psoriasis is an inflammatory autoimmune disorder of the skin, and to treat psoriasis, different nanoformulations (nanoparticles with drugs) were used. The available treatment options for psoriasis are non-specific and associated with systemic toxicity due to the drug and their difficulty associated with deciding the doses.[71] GlyNPs could hold a predictable therapeutic option for treating psoriasis since it is biocompatible, and no additional drugs were used to reduce inflammation. However, the patients are the crucial parameters and extensive research is required with clinical trials. Since the GlyNPs are porous in nature (4–5 nm, see Fig. 1(c) and (e)), many small anti-inflammatory drug molecules can be loaded into them. Furthermore, GlyNPs can be easily internalized by the cells (Fig. 3). These facilities of GlyNPs could be advantageous for targeted delivery to the inflammation-specific cells or to the macrophages to secrete different levels of inflammatory markers and subsequently the inflammation can be reduced through the synergetic effects of GlyNPs and anti-inflammatory drug molecules. Further research has been considered to address all these issues and establish great success with clinical significance.

5. Conclusions

Inflammation causes various diseases, including chronic tissue injury, which demands medicines suitable for the existing therapeutic options. In this work, glycine and acryloyl-based polymeric nanoparticles, GlyNPs, have been synthesized, which provide excellent anti-inflammatory properties. Detailed cell-based studies conclude that these GlyNPs are biocompatible, and studies on macrophages' immunological response are commendable. Network pharmacology and *in silico* studies revealed that these GlyNPs possess target-specific immunomodulatory effects and potential for treating inflammatory diseases. Additionally, RT-PCR analysis revealed the downregulation of specified pro-inflammatory cytokines in support of the anti-inflammatory activities of GlyNPs. Thus, network pharmacology, *in silico*, *in vitro* and *in vivo* studies revealed that GlyNPs are an excellent target-specific immunomodulatory agent, which can also be potentially used for targeted drug delivery and could be an alternate therapeutic for treating acute inflammatory diseases like RA. Furthermore, a detailed study with extensive sampling is required, followed by clinical trials. Any potential anti-inflammatory drug can also be loaded in GlyNPs to form a nanoformulation, which may synergistically reduce inflammation and be useful for treating various inflammatory diseases. To address all the issues related to inflammation and to establish great success in treatment with clinical significance, further research has been taken into consideration.

Author contributions

P. Paik is the principal project investigator (PI). Ideation, experimental design, experimental results analysis, and manuscript writing performed by D. Pareek and P. Paik. Characterization helped by S. Patra, G. Singh, K. Wasnik, and P. S. Gupta. Molecular docking, helped by O. Alagu. *In vivo* work helped by Md. Zeyaullah. Manuscript written and finalized by D. Pareek and P. Paik. All the authors checked and approved the manuscript for publication.

Data availability

All the original data will be available with this article's communicating author and will be provided as required.

Conflicts of interest

The authors have no conflicts of interest to declare.

Acknowledgements

The authors acknowledge the financial support awarded to Prof. Paik by the I-DAPT foundation (ref. I-DAPT/IT (BHU)/2023-24/Project Sanction/47), Indian Council of Medical Research (ICMR), India (Ref: EMDR/SG/12/2023-4724), STARS-IISc. Bangalore (ref. MoE-STARS/STARS-2/2023-0318) and Anusandhan National Research Foundation (ANRF), India (ref: CRG/2023/005576). D. Pareek acknowledges the DST-INSPIRE fellowship awarded to carry out the PhD work (ref. IF 180928).

References

1 E. R. Brannon, M. V. Guevara, N. J. Pacifici, J. K. Lee, J. S. Lewis and O. Eniola-Adefeso, *Nat. Rev. Mater.*, 2022, **7**, 796–813.
2 I. B. McInnes and E. M. Gravallese, *Nat. Rev. Immunol.*, 2021, **21**, 680–686.
3 G. Y. Chen and G. Nuñez, *Nat. Rev. Immunol.*, 2010, **10**, 826–837.
4 E. Kolaczkowska and P. Kubes, *Nat. Rev. Immunol.*, 2013, **13**, 159–175.

5 J. Khambhati, M. Engels, M. Allard-Ratick, P. B. Sandesara, A. A. Quyyumi and L. Sperling, *Atherosclerosis*, 2018, **276**, 1–9.
6 P. Kong, Z.-Y. Cui, X.-F. Huang, D.-D. Zhang, R.-J. Guo and M. Han, *Signal Transduction Targeted Ther.*, 2022, **7**, 131.
7 R. B. Kargbo, *ACS Med. Chem. Lett.*, 2024, **15**, 758–760.
8 G. Monteleone, A. Moscardelli, A. Colella, I. Marafini and S. Salvatori, *Autoimmun. Rev.*, 2023, **22**, 103410.
9 K. F. Baker and J. D. Isaacs, *Ann. Rheum. Dis.*, 2018, **77**, 175.
10 D. Wu, Y. Jin, Y. Xing, M. D. Abate, M. Abbasian, M. Abbasi-Kangevari, Z. Abbasi-Kangevari, F. Abd-Allah, M. Abdelmasseh, M.-A. Abdollahifar, D. M. Abdulah, A. Abedi, V. Abedi, H. Abidi, R. G. Aboagye, H. Abolhassani, K. Abuabara, M. Abyadeh, I. Y. Addo, K. N. Adeniji, A. V. Adepoju, M. A. Adesina, Q. E. Sakilah Adnani, M. Afarideh, S. Aghamiri, A. Agodi, A. Agrawal, C. E. Aguilera Arriagada, A. Ahmad, D. Ahmad, S. Ahmad, S. Ahmad, A. Ahmadi, A. Ahmed, A. Ahmed, J. P. Aithala, A. A. Ajadi, M. Ajami, M. Akbarzadeh-Khiavi, F. Alahdab, M. T. AlBataineh, S. Alemi, A. A. Saeed Al-Gheethi, L. Ali, S. M. Alif, J. U. Almazan, S. Almustanyir, J. S. Alqahtani, I. Alqasmi, I. U. Khan Altaf, N. Alvis-Guzman, N. J. Alvis-Zakzuk, Y. M. Al-Worafi, H. Aly, R. Amani, H. Amu, G. A. Amusa, C. L. Andrei, A. Ansar, H. Ansariniya, A. E. Anyasodor, J. Arabloo, R. Arefnezhad, J. Arulappan, M. Asghari-Jafarabadi, T. Ashraf, J. A. Atata, S. S. Athari, D. Atlaw, M. M. d Wahbi Atout, A. Aujayeb, A. T. Awan, H. Ayatollahi, S. Azadnajafabad, A. Y. Azzam, A. Badawi, A. D. Badiye, S. Bagherieh, A. A. Baig, B. B. Bantie, M. Barchitta, M. Bardhan, S. L. Barker-Collo, F. Barone-Adesi, K. Batra, N. S. Bayileyegn, A. H. Behnoush, U. I. Belgaumi, M. Bemanalizadeh, I. M. Bensenor, K. A. Beyene, A. S. Bhagavathula, P. Bhardwaj, S. Bhaskar, A. N. Bhat, S. Bitaraf, V. R. Bitra, A. Boloor, K. Bora, J. S. Botelho, R. Buchbinder, D. Calina, L. A. Cámera, A. F. Carvalho, J. S. Kai Chan, V. K. Chattu, E. C. Abebe, F. Chichagi, S. Choi, T.-C. Chou, D.-T. Chu, K. Coberly, V. M. Costa, R. A. S. Couto, N. Cruz-Martins, O. Dadras, X. Dai, G. Damiani, A. M. Dascalu, M. Dashti, S. A. Debela, R. P. Dellavalle, A. K. Demetriades, A. A. Demlash, X. Deng, H. D. Desai, R. Desai, S. M. Rahman Dewan, S. Dey, S. D. Dharmaratne, D. Diaz, M. Dibas, R. J. Dinis-Oliveira, M. Diress, T. C. Do, D. K. Doan, M. Dodangeh, M. Dodangeh, D. Dongarwar, J. Dube, A. M. Dziedzic, A. Ed-Dra, H. A. Edinur, N. Eissazade, M. Ekholuenetale, T. C. Ekundayo, N. M. Elemam, M. Elhadi, A. O. Elmehrath, O. A. Abdou Elmeligy, M. Emamverdi, T. I. Emeto, H. L. Esayas, H. B. Eshetu, F. Etaee, A. F. Fagbamigbe, S. Faghani, I. R. Fakhradiyev, A. Fatehizadeh, M. Fathi, A. Feizkhah, G. Fekadu, M. Fereidouni, S.-M. Fereshtehnejad, J. C. Fernandes, P. Ferrara, G. Fetensa, I. Filip, F. Fischer, B. Foroutan, M. Foroutan, T. Fukumoto, B. Ganesan, B. N. Belete Gemeda, S.-H. Ghamari, M. Ghasemi, M. Gholamalizadeh, T. K. Gill, R. F. Gillum, M. Goldust, M. Golechha, P. Goleij, D. Golinelli, H. Goudarzi, S.-Y. Guan, Y. Guo, B. Gupta, V. B. Gupta, V. K. Gupta, R. Haddadi, N. R. Hadi, R. Halwani, S. Haque, I. Hasan, R. Hashempour, A. Hassan, T. S. Hassan, S. Hassanzadeh, M. B. Hassen, J. Haubold, K. Hayat, G. Heidari, M. Heidari, R. Heidari-Soureshjani, C. Herteliu, K. Hessami, K. Hezam, Y. Hiraike, R. Holla, M.-S. Hosseini, H.-H. Huynh, B.-F. Hwang, S. E. Ibitoye, I. M. Ilic, M. D. Ilic, A. Iranmehr, F. Iravanpour, N. E. Ismail, M. Iwagami, C. C. D. Iwu, L. Jacob, M. Jafarinia, A. Jafarzadeh, K. Jahankhani, H. Jahrami, M. Jakovljevic, E. Jamshidi, C. T. Jani, M. D. Janodia, S. K. Jayapal, S. Jayaram, J. Jeganathan, J. B. Jonas, A. Joseph, N. Joseph, C. E. Joshua, K. Vaishali, B. Kaambwa, A. Kabir, Z. Kabir, V. Kadashetti, F. Kaliyadan, F. Kalroozi, V. K. Kamal, A. Kandel, H. Kandel, S. Kanungo, J. Karami, I. M. Karaye, H. Karimi, H. Kasraei, S. Kazemian, S. A. Kebede, L. Keikavoosi-Arani, M. Keykhaei, Y. S. Khader, H. Khajuria, F. Khamesipour, E. A. Khan, I. A. Khan, M. Khan, M. J. Khan, M. A. B. Khan, M. A. Khan, H. Khatatbeh, M. M. Khatatbeh, S. Khateri, H. R. Khayat Kashani, M. S. Kim, A. Kisa, S. Kisa, H. Y. Koh, P. Kolkhir, O. Korzh, A. L. Kotnis, P. A. Koul, A. Koyanagi, K. Krishan, M. Kuddus, V. V. Kulkarni, N. Kumar, S. Kundu, O. P. Kurmi, C. La Vecchia, C. Lahariya, T. Laksono, J. Lám, K. Latief, P. Lauriola, B. K. Lawal, T. T. Thu Le, T. T. Bich Le, M. Lee, S. W. Lee, W.-C. Lee, Y. H. Lee, J. Lenzi, M. Levi, W. Li, V. S. Ligade, S. S. Lim, G. Liu, X. Liu, E. Llanaj, C.-H. Lo, V. S. Machado, A. A. Maghazachi, M. A. Mahmoud, T. A. Mai, A. Majeed, P. M. Sanaye, O. M. Makram, E. M. Rad, K. Malhotra, A. A. Malik, I. Malik, T. H. Mallhi, D. C. Malta, M. A. Mansournia, L. G. Mantovani, M. Martorell, S. Masoudi, S. Z. Masoumi, Y. Mathangasinghe, E. Mathews, A. G. Mathioudakis, A. Maugeri, M. Mayeli, J. R. Carabeo Medina, G. G. Meles, J. J. Mendes, R. G. Menezes, T. Mestrovic, I. M. Michalek, A. C. Micheletti Gomide Nogueira de Sá, E. T. Mihretie, L. H. Nhat Minh, R. Mirfakhraie, E. M. Mirrakhimov, A. Misganaw, A. Mohamadkhani, N. S. Mohamed, F. Mohammadi, S. Mohammadi, S. Mohammed, S. Mohammed, S. Mohan, A. Mohseni, A. H. Mokdad, S. Momtazmanesh, L. Monasta, M. A. Moni, M. Moniruzzaman, Y. Moradi, N. Morovatdar, E. Mostafavi, P. Mousavi, G. D. Mukoro, A. Mulita, G. B. Mulu, E. Murillo-Zamora, F. Musaigwa, G. Mustafa, S. Muthu, F. Nainu, V. Nangia, S. N. Swamy, Z. S. Natto, P. Navaraj, B. P. Nayak, A. Nazri-Panjaki, H. Negash, M. H. Nematollahi, D. H. Nguyen, H. T. Hien Nguyen, H. Q. Nguyen, P. T. Nguyen, V. T. Nguyen, R. K. Niazi, T. K. Nikolouzakis, L. A. Nnyanzi, M. Noreen, C. I. Nzoputam, O. J. Nzoputam, B. Oancea, I.-H. Oh, H. Okati-Aliabad, O. C. Okonji, P. G. Okwute, A. T. Olagunju, M. I. Olatubi, I. I. Olufadewa, M. Ordak, N. Otstavnov, M. O. Owolabi, P. A. Mahesh, J. R. Padubidri, A. Pak, R. Pakzad, R. Palladino, A. Pana, I. Pantazopoulos, P. Papadopoulou, S. Pardhan, A. Parthasarathi, A. Pashaei, J. Patel, A. R. Pathan, S. Patil, U. Paudel, S. Pawar, P. Pedersini, U. Pensato, D. M. Pereira, J. Pereira, M. O. Pereira, R. B. Pereira, M. F. P. Peres, A. Perianayagam, S. Perna, I.-R. Petcu, P. S. Pezeshki, H. T. Pham, A. K. Philip, M. A. Piradov, I. Podder, V. Podder, D. Poddighe, E. J. Sady Prates,

I. Qattea, A. Radfar, P. Raee, A. Rafiei, A. Raggi, F. Rahim, M. Rahimi, M. Rahimifard, V. Rahimi-Movaghar, M. O. Rahman, M. H. Ur Rahman, M. Rahman, M. A. Rahman, A. M. Rahmani, M. Rahmani, S. Rahmani, V. Rahmanian, P. Ramasubramani, N. Rancic, I. R. Rao, S. Rashedi, A. M. Rashid, N. Ravikumar, S. Rawaf, E. M. Mohamed Redwan, N. Rezaei, N. Rezaei, N. Rezaei, M. Rezaeian, D. Ribeiro, M. Rodrigues, J. A. Buendia Rodriguez, L. Roever, E. Romero-Rodríguez, A. M. A. Saad, B. Saddik, S. Sadeghian, U. Saeed, A. Safary, M. Safdarian, S. Z. Safi, A. Saghazadeh, D. Sagoe, F. S. Sharif-Askari, N. S. Sharif-Askari, A. Sahebkar, H. Sahoo, M. A. Sahraian, M. R. Sajid, S. Sakhamuri, J. W. Sakshaug, M. A. Saleh, L. Salehi, S. Salehi, A. S. Farrokhi, S. Samadzadeh, S. Samargandy, N. Samieefar, A. M. Samy, N. Sanadgol, R. K. Sanjeev, M. Sawhney, G. K. Saya, A. Schuermans, S. Senthilkumaran, S. G. Sepanlou, Y. Sethi, M. Shafie, H. Shah, I. Shahid, S. Shahid, M. A. Shaikh, S. Sharfaei, M. Sharma, M. Shayan, H. S. Shehata, A. Sheikh, J. K. Shetty, J. I. Shin, R. Shirkoohi, N. A. Shitaye, K. M. Shivakumar, V. Shivarov, P. Shobeiri, S. Siabani, M. M. Sibhat, E. E. Siddig, C. R. Simpson, E. Sinaei, H. Singh, I. Singh, J. A. Singh, P. Singh, S. Singh, M. S. Siraj, A. Al Mamun Sohag, R. Solanki, S. Solikhah, Y. Solomon, M. S. Soltani-Zangbar, J. Sun, M. D. Szeto, R. Tabarés-Seisdedos, S. M. Tabatabaei, M. Tabish, E. Taheri, A. Tahvildari, I. M. Talaat, J. J. L. Lukenze Tamuzi, K.-K. Tan, N. Y. Tat, R. T. Oliaee, A. Tavasol, M.-H. Temsah, P. Thangaraju, S. Tharwat, N. S. Tibebu, J. H. Vera Ticoalu, T. Tillawi, T. Y. Tiruye, A. Tiyuri, M. R. Tovani-Palone, M. Tripathi, G. M. Tsegay, A. R. Tualeka, S. S. Ty, C. S. Ubah, S. Ullah, S. Ullah, M. Umair, S. Umakanthan, E. Upadhyay, S. M. Vahabi, A. G. Vaithinathan, S. V. Tahbaz, R. Valizadeh, S. B. Varthya, T. J. Vasankari, N. Venketasubramanian, G.-I. Verras, J. H. Villafañe, V. Vlassov, D. C. Vo, Y. Waheed, A. Waris, B. G. Welegebrial, R. Westerman, D. P. Wickramasinghe, N. D. Wickramasinghe, B. Willekens, B. Z. Woldegeorgis, M. Woldemariam, H. Xiao, D. Y. Yada, G. Yahya, L. Yang, F. Yazdanpanah, D. K. Yon, N. Yonemoto, Y. You, M. Zahir, S. S. Zaidi, M. Zangiabadian, I. Zare, M. A. Zeineddine, D. T. Zemedikun, N. G. Zeru, C. Zhang, H. Zhao, C. Zhong, M. Zielińska, M. Zoladl, A. Zumla, C. Guo and L.-S. Tam, *eClinicalMedicine*, 2023, **64**, 102193.

11 E. Alexander and K. W. Leong, *J. Nanobiotechnol.*, 2024, **22**, 661.

12 Y. Huang, X. Guo, Y. Wu, X. Chen, L. Feng, N. Xie and G. Shen, *Signal Transduction Targeted Ther.*, 2024, **9**, 34.

13 A. K. Mishra, L. Rani, R. Singh, H. K. Dewangan, P. K. Sahoo and V. Kumar, *J. Drug Delivery Sci. Technol.*, 2024, **93**, 105446.

14 R. Brusini, M. Varna and P. Couvreur, *Adv. Drug Delivery Rev.*, 2020, **157**, 161–178.

15 R. Mohammapdour and H. Ghandehari, *Adv. Drug Delivery Rev.*, 2022, **180**, 114022.

16 F. A. Waliaveettil, J. Jose and E. I. Anila, *ACS Appl. Bio Mater.*, 2025, **9**(1), 628–641.

17 H. Jeong, K. Subramanian, J.-B. Lee, H. Byun, H. Shin and J.-H. Yun, *Biomater. Sci.*, 2025, **13**, 810–825.

18 C. M. A. van Alem, M. Boonstra, J. Prins, T. Bezhaeva, M. F. van Essen, J. M. Ruben, A. L. Vahrmeijer, E. P. van der Veer, J. W. de Fijter, M. E. Reinders, O. Meijer, J. M. Metselaar, C. van Kooten and J. I. Rotmans, *Nephrol., Dial., Transplant.*, 2018, **33**, 44–53.

19 M. Zhou, J. Hou, Z. Zhong, N. Hao, Y. Lin and C. Li, *Drug Delivery*, 2018, **25**, 716–722.

20 Y. Karabey-Akyurek, A. G. Gurcay, O. Gurcan, O. F. Turkoglu, S. Yabanoglu-Ciftci, H. Eroglu, M. F. Sargon, E. Bilensoy and L. Oner, *Pharm. Dev. Technol.*, 2017, **22**, 972–981.

21 Q. Wang, J. Jiang, W. Chen, H. Jiang, Z. Zhang and X. Sun, *J. Controlled Release*, 2016, **230**, 64–72.

22 R. L. Bartlett, S. Sharma and A. Panitch, *Nanomedicine*, 2013, **9**, 419–427.

23 R. M. Gonçalves, A. C. L. Pereira, I. O. Pereira, M. J. Oliveira and M. A. Barbosa, *J. Mater. Sci.: Mater. Med.*, 2015, **26**, 167.

24 Y.-C. Chen, S. F. Gad, D. Chobisa, Y. Li and Y. Yeo, *J. Controlled Release*, 2021, **330**, 438–460.

25 P. S. Gupta, K. Wasnik, G. Singh, S. Patra, D. Pareek, D. D. Yadav, M. S. Tomar, S. Maiti, M. Singh and P. Paik, *Mater. Adv.*, 2023, **4**, 4718–4731.

26 P. S. Gupta, K. Wasnik, S. Patra, D. Pareek, G. Singh, D. D. Yadav, S. Maity and P. Paik, *Nanoscale*, 2024, **16**, 1770–1791.

27 J. Pietsch, S. Riwaldt, J. Bauer, A. Sickmann, G. Weber, J. Grosse, M. Infanger, C. Eilles and D. Grimm, *Int. J. Mol. Sci.*, 2013, **14**, 1164–1178.

28 T. Liu, L. Zhang, D. Joo and S.-C. Sun, *Signal Transduction Targeted Ther.*, 2017, **2**, 17023.

29 J. Tuncel, S. Haag, M. H. Hoffmann, A. C. Y. Yau, M. Hultqvist, P. Olofsson, J. Bäcklund, K. S. Nandakumar, D. Weidner, A. Fischer, A. Leichsenring, F. Lange, C. Haase, S. Lu, P. S. Gulko, G. Steiner and R. Holmdahl, *PLoS One*, 2016, **11**, e0155936.

30 A. K. Yamala, V. Nadella, Y. Mastai, H. Prakash and P. Paik, *Nanoscale*, 2017, **9**, 14006–14014.

31 N. Lewinski, V. Colvin and R. Drezek, *Small*, 2008, **4**, 26–49.

32 S. X. Ge, D. Jung and R. Yao, *Bioinformatics*, 2020, **36**, 2628–2629.

33 G. M. Morris and M. Lim-Wilby, in *Molecular Modeling of Proteins*, ed. A. Kukol, Humana Press, Totowa, NJ, 2008, pp. 365–382, DOI: **10.1007/978-1-59745-177-2_19**.

34 P. Mark Andrew, A. S. Marisa, L. W. Darby and X. Zhong-Ru, in *Molecular Docking*, ed. P. V. Dimitrios, IntechOpen, Rijeka, 2018, ch. 8, DOI: **10.5772/intechopen.72898**.

35 P. C. Agu, C. A. Afiukwa, O. U. Orji, E. M. Ezeh, I. H. Ofoke, C. O. Ogbu, E. I. Ugwuja and P. M. Aja, *Sci. Rep.*, 2023, **13**, 13398.

36 U. Lo, V. Selvaraj, J. M. Plane, O. V. Chechneva, K. Otsu and W. Deng, *Sci. Rep.*, 2014, **4**, 7405.

37 Q. Guo, Y. Jin, X. Chen, X. Ye, X. Shen, M. Lin, C. Zeng, T. Zhou and J. Zhang, *Signal Transduction Targeted Ther.*, 2024, **9**, 53.

38 C. H. Evans, *Agents Actions Suppl.*, 1995, **47**, 107–116.

39 J. N. Sharma, A. Al-Omran and S. S. Parvathy, *Inflammopharmacology*, 2007, **15**, 252–259.

40 C. Wang, R. Rao, Z. Cai, H. Yang, L. Zhang, S. Ji, C. Zhang, D. Gao, Y. Hu, J. Li, W. Xiong, H. Jiang, J. Chu and D. Wu, *ACS Nano*, 2023, **17**, 9025–9038.
41 J. Yeo, Y. M. Lee, J. Lee, D. Park, K. Kim, J. Kim, J. Park and W. J. Kim, *Nano Lett.*, 2019, **19**, 6716–6724.
42 Y. Oh, H. Jeong, S. Lim and J. Hong, *Biomacromolecules*, 2020, **21**, 4972–4979.
43 Z. Strizova, I. Benesova, R. Bartolini, R. Novysedlak, E. Cecrdlova, L. K. Foley and I. Striz, *Clin. Sci.*, 2023, **137**, 1067–1093.
44 M. I. Edilova, A. Akram and A. A. Abdul-Sater, *Biomed. J.*, 2021, **44**, 172–182.
45 J. S. Smolen, D. Aletaha, A. Barton, G. R. Burmester, P. Emery, G. S. Firestein, A. Kavanaugh, I. B. McInnes, D. H. Solomon, V. Strand and K. Yamamoto, *Nat. Rev. Dis. Primers*, 2018, **4**, 18001.
46 J. E. Pope and E. H. Choy, *Semin. Arthritis Rheum.*, 2021, **51**, 219–229.
47 C. Ciurtin, G. A. Helmy, A. C. Ferreira, J. J. Manson, E. C. Jury and T. McDonnell, *Clin. Immunol.*, 2024, **265**, 110281.
48 D. S. Pisetsky and P. E. Lipsky, *Nat. Rev. Rheumatol.*, 2020, **16**, 565–579.
49 S. S. Paknikar, C. S. Crowson, J. M. Davis and U. Thanarajasingam, *ACR Open Rheumatol.*, 2021, **3**, 422–426.
50 A. Kavanaugh, R. Tomar, J. Reveille, D. H. Solomon and H. A. Homburger, *Arch. Pathol. Lab. Med.*, 2000, **124**, 71–81.
51 Z. F. Mahdi, S. H. Mohammed and A. R. Hadi, *Al-Rafidain J. Med. Sci.*, 2023, **5**, 105–111.
52 G. Steiner and J. Smolen, *Arthritis Res. Ther.*, 2002, **4**, S1.
53 D. Alkhudir, A. Al-Herz, K. Saleh, A. Alawadhi, W. Al-Kandari, E. Hasan, K. Mokaddem, A. Ghanem, Y. A. Bartella, M. Hussain, N. AlHadhood, Y. Ali, E. Nahar, A. Alenizi, A. Aldei, F. Abutiban, S. Hayat, H. Behbehani, F. Baron, H. Alhajeri, A. Alkadi and A. Alsaber, *Open Access Rheumatol.: Res. Rev.*, 2023, **15**, 223–230.
54 N. Caronni, F. La Terza, F. M. Vittoria, G. Barbiera, L. Mezzanzanica, V. Cuzzola, S. Barresi, M. Pellegatta, P. Canevazzi, G. Dunsmore, C. Leonardi, E. Montaldo, E. Lusito, E. Dugnani, A. Citro, M. S. F. Ng, M. Schiavo Lena, D. Drago, A. Andolfo, S. Brugiapaglia, A. Scagliotti, A. Mortellaro, V. Corbo, Z. Liu, A. Mondino, P. Dellabona, L. Piemonti, C. Taveggia, C. Doglioni, P. Cappello, F. Novelli, M. Iannacone, L. G. Ng, F. Ginhoux, S. Crippa, M. Falconi, C. Bonini, L. Naldini, M. Genua and R. Ostuni, *Nature*, 2023, **623**, 415–422.
55 S. Pasi, R. Kant, S. Gupta and A. Surolia, *Biomaterials*, 2015, **42**, 121–133.
56 M. Adachi, S. Okamoto, S. Chujyo, T. Arakawa, M. Yokoyama, K. Yamada, A. Hayashi, K. Akita, M. Takeno, S. Itoh, T. Takii, Y. Waguri-Nagaya, T. Otsuka, K. Hayakawa, K. Miyazawa and K. Onozaki, *J. Interferon Cytokine Res.*, 2013, **33**, 297–307.
57 G. van Loo and M. J. M. Bertrand, *Nat. Rev. Immunol.*, 2023, **23**, 289–303.
58 D.-i Jang, A. H. Lee, H.-Y. Shin, H.-R. Song, J.-H. Park, T.-B. Kang, S.-R. Lee and S.-H. Yang, *Int. J. Mol. Sci.*, 2021, **22**, 2719.
59 D. Furman, J. Campisi, E. Verdin, P. Carrera-Bastos, S. Targ, C. Franceschi, L. Ferrucci, D. W. Gilroy, A. Fasano, G. W. Miller, A. H. Miller, A. Mantovani, C. M. Weyand, N. Barzilai, J. J. Goronzy, T. A. Rando, R. B. Effros, A. Lucia, N. Kleinstreuer and G. M. Slavich, *Nat. Med.*, 2019, **25**, 1822–1832.
60 V. P. Chavda, J. Feehan and V. Apostolopoulos, *Cells*, 2024, **13**(22), 1906.
61 Y. Huang, J. Xu, G. Sun, X. Cheng, Y. An, X. Yao, G. Nie and Y. Zhang, *Biomaterials*, 2025, **314**, 122822.
62 J. E. Karbowniczek, K. Berniak, J. Knapczyk-Korczak, G. Williams, J. A. Bryant, N. D. Nikoi, M. Banzhaf, F. de Cogan and U. Stachewicz, *J. Colloid Interface Sci.*, 2023, **650**, 1371–1381.
63 K. Ernits, C. K. Saha, T. Brodiazhenko, B. Chouhan, A. Shenoy, J. A. Buttress, J. J. Duque-Pedraza, V. Bojar, J. A. Nakamoto, T. Kurata, A. A. Egorov, L. Shyrokova, M. J. O. Johansson, T. Mets, A. Rustamova, J. Džigurski, T. Tenson, A. Garcia-Pino, H. Strahl, A. Elofsson, V. Hauryliuk and G. C. Atkinson, *Proc. Natl. Acad. Sci. U. S. A.*, 2023, **120**, e2305393120.
64 K. Wasnik, P. S. Gupta, S. Mukherjee, A. Oviya, R. Prakash, D. Pareek, S. Patra, S. Maity, V. Rai, M. Singh, G. Singh, D. D. Yadav, S. Das, P. Maiti and P. Paik, *ACS Appl. Bio Mater.*, 2023, **6**, 5644–5661.
65 N. H. Evans and P. D. Beer, *Angew. Chem., Int. Ed.*, 2014, **53**, 11716–11754.
66 C. S. L. Tuttle, L. A. N. Thang and A. B. Maier, *Ageing Res. Rev.*, 2020, **64**, 101185.
67 Y. Qu, J. Li, Q. Qin, D. Wang, J. Zhao, K. An, Z. Mao, Z. Min, Y. Xiong, J. Li and Z. Xue, *npj Parkinson's Dis.*, 2023, **9**, 18.
68 Q. Wang, X. Qin, J. Fang and X. Sun, *Acta Pharm. Sin. B*, 2021, **11**, 1158–1174.
69 M. Barani, A. Rahdar, S. Sargazi, M. S. Amiri, P. K. Sharma and N. Bhalla, *Sens. Bio-Sens. Res.*, 2021, **32**, 100417.
70 J. Gao, J. Li, Z. Luo, H. Wang and Z. Ma, *Drug Des., Dev. Ther.*, 2024, **18**, 2921–2949.
71 M. Pradhan, A. Alexander, M. R. Singh, D. Singh, S. Saraf, S. Saraf and Ajazuddin, *Biomed. Pharmacother.*, 2018, **107**, 447–463.